# INFORMATION TO USERS

This manuscript has been reproduced from the microfilm master. UMI films the text directly from the original or copy submitted. Thus, some thesis and dissertation copies are in typewriter face, while others may be from any type of computer printer.

The quality of this reproduction is dependent upon the quality of the copy submitted. Broken or indistinct print, colored or poor quality illustrations and photographs, print bleedthrough, substandard margins, and improper alignment can adversely affect reproduction.

In the unlikely event that the author did not send UMI a complete manuscript and there are missing pages, these will be noted. Also, if unauthorized copyright material had to be removed, a note will indicate the deletion.

Oversize materials (e.g., maps, drawings, charts) are reproduced by sectioning the original, beginning at the upper left-hand corner and continuing from left to right in equal sections with small overlaps.

Photographs included in the original manuscript have been reproduced xerographically in this copy. Higher quality 6" x 9" black and white photographic prints are available for any photographs or illustrations appearing in this copy for an additional charge. Contact UMI directly to order.

Bell & Howell Information and Learning
300 North Zeeb Road, Ann Arbor, MI 48106-1346 USA
800-521-0600

# CONTROL OF WALKING IN A QUADRUPED ROBOT WITH STIFF LEGS


## Anca Elena Cocosco

Department of Mechanical Engineering
McGill University, Montréal


July 1998

A Thesis submitted to the Faculty of Graduate Studies and Research
in partial fulfilment of the requirements for the degree of
Master of Engineering

To

my parents

and my husband Andrei

# ABSTRACT

Over half of the earth's dry surface is inaccessible to wheeled or tracked vehicles. Even relatively structured indoor or urban environments with steps, stairs, or narrow hallways, are challenging for most wheeled or tracked systems. This is one of the primary motivations for the study of mobile robots with legs.

We propose a new type of quadruped robot with maximum mechanical simplicity - the SCOUT class. Most robots built to date possess many actuated degrees of freedom (DOF) (three or four per leg) thus making them too expensive for practical use. SCOUT robots, on the other hand, feature only one actuated degree of freedom per leg. SCOUT dynamics, while still non-trivial, is greatly simplified compared to that of higher degree of freedom robots. In our analysis, we assume instantaneous plastic impacts occur when a leg touches the ground, and consequently, a momentum transfer occurs that causes step changes in the linear and angular velocities. The calculations of these changes are based on the principle of conservation of angular momentum with respect to the impact toe, since it is that point which acts as pivot, or a free pin joint. A set of walking algorithms based on the controlled momentum transfer have been developed, and validated, using numerical simulations. These algorithms have subsequently been implemented on our walking robots, SCOUT I and SCOUT II.

This thesis will show that, with very simple mechanical design and control strategies, stable walking is achievable. However, it is important to note that research currently being undertaken in the ARL group will establish that, with only minimal structural changes, SCOUT will have the ability to run and climb stairs.

# RÉSUMÉ

Plus de la moitié de la masse continentale de la Terre est inaccessible aux véhicules à roues ou à chenilles. Même des environnements intérieurs ou urbains relativements structurés représentent un défi pour la plupart des systèmes à roues ou à chenilles. C'est l'une des principales motivations pour l'étude de robots mobiles à jambes.

Nous proposons un nouveau type de robot quadrupède avec une simplicité mécanique maximale - la classe SCOUT. La plupart des robots construits jusqu'ici possèdent beaucoup de degrés de liberté motorisés (trois ou quatre par jambe), ce qui les rend trop cher en pratique. Les robots SCOUT, par contre, n'ont qu'un seul degré de liberté (DDL) motorisé par jambe. La dynamique des SCOUT, tout en restant non triviale, est grandement simplifiée comparée à celle des robots avec plus de degrés de liberté. Dans notre analyse, nous supposons que des impacts plastiques instantanés ont lieu quand une jambe touche le sol, et, par conséquent, un transfer de momentum se produit qui cause un échelon dans les vitesses angulaires et linéaires. Les calculs pour ces changements sont basés sur le principe de conservation du momentum angulaire par rapport au point d'impact, puisque c'est ce point qui agit comme pivot. Un ensemble d'algorithmes de marche, basés sur le commande du transfer du momentum, ont été développés et validés par l'utilisation de simulations numériques. Ces algorithmes ont par la suite été implémentés sur nos robots marchants, SCOUT I et SCOUT II.

Cette thèse montrera que, avec une conception mécanique et des stratégies de contrôle très simples, une marche stable est atteignable. Cependant, il est important de noter que la recherche présentement effectuée au sein du groupe ARL établira que,

avec des changements structuraux minimes, SCOUT aura la capacité de courir et de gravir des escaliers.

# ACKNOWLEDGEMENTS

I would like to first extend my sincere appreciation to my supervisor, Professor Martin Buehler, whose enthusiasm and dedication helped me find joy in my research. Several years ago, when I was an undergrad student eager to learn more, he welcomed me into the wonderful ARL "family" and spent countless hours showing me the true meaning of research. He is much more than a professor to me. He is a mentor - someone who inspired me to pursue graduate studies and who continues to set an example of what dedication and hard work really mean.

I am also thankful to Mojtaba Ahamdi, who provided unconditional help through the course of my research. His encouragement, generosity and willingness to sit down and help me with my thesis demonstrated to me that he is a genuine and valued friend.

All of the people that are, or were, in the Ambulatory Robotics Laboratory (ARL) influenced my research: Gregory Petryk and John Damianakis, for encouraging my dreams when I was just a "kid" in the lab; Katja Dauster for bringing me chocolates when I needed a sugar boost; Sami Obaid for his cheerfulness and his enthusiasm; Robert Battaglia for his tremendous help with the experimental setup and for providing me with some of the drawings included in this thesis; Dave McMordie for his help in debugging the electronic hardware; Mike Glaum, the expert in control theories, for helping me understand control concepts; Pierre Montagnier, for not getting angry at me for always knocking on his door in my search for Mojtaba and for providing me with the French translation of the abstract. And last, but not least Ken Yamazaki, whose help in so many ways had such a positive influence on my research.

I would also like to thank all of the CIM (Center of Intelligent Machines) staff: Kathleen VanderNoot and Ornella Cavaliere for making sure that we always had everything we needed and that we also had some fun together. My deepest thanks to our manager, Marlene Gray, who read the first draft of this thesis and provided guidance to me in improving the quality of my writing.

Finally ... my family. My mother and father whose devotion while raising me and my brother made me the person that I am today. Without their support, encouragement and tremendous sacrifice, my life would have been very different. They gave me the chance to realize a dream. Special thanks to my brother, whose excellent school records motivated me to achieve the highest standards possible. And finally, words can never describe my feelings toward my husband Andrei; his unwavering support and understanding made everything possible and easy. It was his love and appreciation that kept me going even when "mother science" humbled me by showing that I still make mistakes. Thank you Andrei!

# TABLE OF CONTENTS

# LIST OF FIGURES

# LIST OF TABLES

# CHAPTER 1

# INTRODUCTION

## 1.1. Motivation

Humans and legged animals can move quickly and easily over soft, hard or difficult terrain, such as mountains, valleys, craters and crevices. The hope is that legged robots with similar dexterity as their biological counterparts perform better over these types of surfaces than wheeled or tracked machines. Legged robots are needed in a variety of fields: land or space exploration, surveillance or work in dangerous environments, police operations, forestry, civil and medical applications and even the entertainment industry. In most applications, a legged robot should either provide a means of locomotion or take over the human role, particularly where the use of humans would be expensive, dangerous, or occasionally, impossible. The applications for legged robots involve activities which pose a significant challenge to a wheeled or tracked vehicle, such as running, climbing or descending stairs, walking on rocky terrain and passing or jumping over obstacles. However, current research in legged robotics is still in its infancy, and, therefore, has a long way to go in building practical dextrous and agile legged robots which can successfully and effectively deal with various types of terrain.

## 1.2. Research on Legged Locomotion

Legged robots generally fall into two classes; those designed for static walking and those capable of dynamic operation. In static walkers, stability is assured through kinematics by keeping the machine's center of mass within the polygon formed by the supporting feet. This requires that these machines have at least four legs, although they are often built with six legs to improve mobility. Static walkers do not balance actively and, since dynamics of motion are not considered, speeds are low in comparison with the performances obtained by the dynamic walkers of the same leg length.

Dynamic operation requires that balance is actively maintained at all times. Dynamic robots have a potential for higher speeds and power efficiency. Moreover, they require fewer legs, and consequently simpler designs. Unlike statically stable robots, which operate around the equilibrium position, the actively balanced robots can operate away from the static equilibrium configuration, with a direct consequence on an increased mobility. Due to their agility, dynamic legged robots can move more easily around different obstacles or can negotiate a larger variety of terrains.

Important research in dynamically stable locomotion was developed by Raibert who started with a one legged hopping robot and went on to build various bipeds and a quadruped [**16**]. The concepts developed for the one legged robot were used in the control of the three dimensional biped and the quadruped robot. Miura and Shimoyama [**15**] developed the BIPER family of statically unstable biped robots that perform dynamically stable walking. Channon, Hopkins, and Pham [**3**] presented alternative ways of designing walking algorithms using optimization techniques. The same idea was used by Kajita, Tani, and Kobayashi [**7**] in designing a potential energy conserving trajectory for their biped robot. The design of the walking gait based on energy minimization was used also by Marhefka and Orin [**10**]. Dunn and Howe [**4, 5**] analyzed the smooth motion, with constant body height, of a bipedal robot. During the leg impacts, the angular momentum of the entire machine about the impacting leg is conserved. The same conservation principle was used by McGeer [**11, 12, 13**] in

his analysis of a bipedal locomotion, by Smith and Berkemeier [**19**] in their research on quadrupedal walking, and by Sano and Furusho [**18**] in designing walking gaits for the BLR-G2 biped. So far, the research on dynamically stable robots proved the important effect of impacts, and the use of these impacts in maintaining a walking motion.

## 1.3. SCOUT legged robots

FIGURE 1.1. Photos of SCOUT I (left) and SCOUT II (right)

A review of the available legged robots indicates that these machines are sophisticated and quite expensive. In contrast, we aimed at a low cost, mechanically simple machine - the SCOUT robots (Figure 1.1). Despite the design constraints, our robot should still be able to perform walking, running and stair climbing tasks. Two generations of SCOUT robots (Figure 1.1) have been designed and built in the Ambulatory Robotics Laboratory (ARL). According to the design requirements, SCOUT has a very simple structure featuring only one degree of freedom (DOF) per leg.

Current research conducted in the ARL group is focused on designing control algorithms for walking, running, and stair climbing, as well as improvements in the mechanical design. Ken Yamazaki built the first prototype, SCOUT I, and designed

and implemented successfully the first walking controller on SCOUT I. This thesis will present control algorithms designed for walking gaits. Moreover, some of the presented algorithms were implemented on SCOUT II, and the experimental results will show the performance of the walking controllers. Robert Battaglia designed and built SCOUT II and currently is developing algorithms for stair climbing. Joseph Sarkis designed control schemes for running gaits. Sami Obaid equipped SCOUT II with two triangulation laser proximity sensors used for different sensing tasks. The third generation of SCOUT robots is already being researched: Geoff Hawker is analyzing the behavior of SCOUT equipped with legs with unactuated knees.

This thesis is dedicated to the design and analysis of walking control algorithms. We consider the motion in the sagittal plane where the back legs act in unison, as do the front legs. The analysis of the walking gait will prove, via simulations and experiments, that using the conservation of angular momentum of the system around the impact leg, it is possible to develop simple control algorithms that yield stable walking.

## 1.4. Contributions

- The kinematic and dynamic model of SCOUT will be derived and validated via the MOBILE [**8**] simulation package (Section 2.2).
- The kinematic momentum model that governs the impact of a leg will be developed and validated via the WORKING MODEL [**17**] simulation package (Section 2.3).
- Three different control schemes will be proposed and validated via numerical simulations. A numerical stability analysis will be included in the study of the proposed controllers (Chapter 3).
- Two walking controllers have been implemented experimentally on the SCOUT II robot (Chapter 4).

## 1.5. Terminology

The following terms will be used throughout this thesis:

- *back leg*: leg representing the pairwise motion of the two back (with respect to the direction of motion) legs
- *front leg*: leg representing the pairwise motion of the two front legs
- *back leg support*: SCOUT is supported only by the back leg
- *front leg support*: SCOUT is supported only by the front leg
- *single stance*: either back leg or front leg are in contact with the ground
- *double stance*: both back and front leg are in contact with the ground
- *step*: the succession of back leg support, front leg impact, front leg support and back leg impact
- *turn over*: the robot falls backwards or head over forwards and lands on its back

## 1.6. Organization of the Thesis

Chapter 2 derives the mathematical model governing the SCOUT motion in single stance and the model governing the back leg or front leg toe impact. Chapter 3 presents the three proposed control strategies together with their numerical stability analyses. Chapter 4 shows experimental results obtained from the implementation of two controllers on SCOUT II and Chapter 5 summarizes the results of our research and presents some recommendations for future work.

# CHAPTER 2

# MATHEMATICAL MODEL

## 2.1. Modeling Considerations

This thesis is dedicated to the design and analysis of walking algorithms. The analysis will be done via computer simulations which will require a mathematical system model. In modeling the system we made several simplifying assumptions:

- SCOUT has only planar motion; therefore, our model has only one back leg and one front leg;
- the legs are rigid and massless;
- the joints are friction-less ;
- when the toes are in contact with the ground, they behave as free, friction-less pin connections (the toes do not slip on the ground).

Figure 2.1 shows a schematics of our model. The body is connected to the legs through friction-less rotational joints, the back and front *hips* ($H_b$, $H_f$). The *virtual leg* ($l_b$, $l_f$ in Figure 2.1) is a virtual element connecting the toe ($T_b$, $T_f$) to the body center of mass (C). The actuators are placed at the hips ($H_b$, $H_f$), and control the

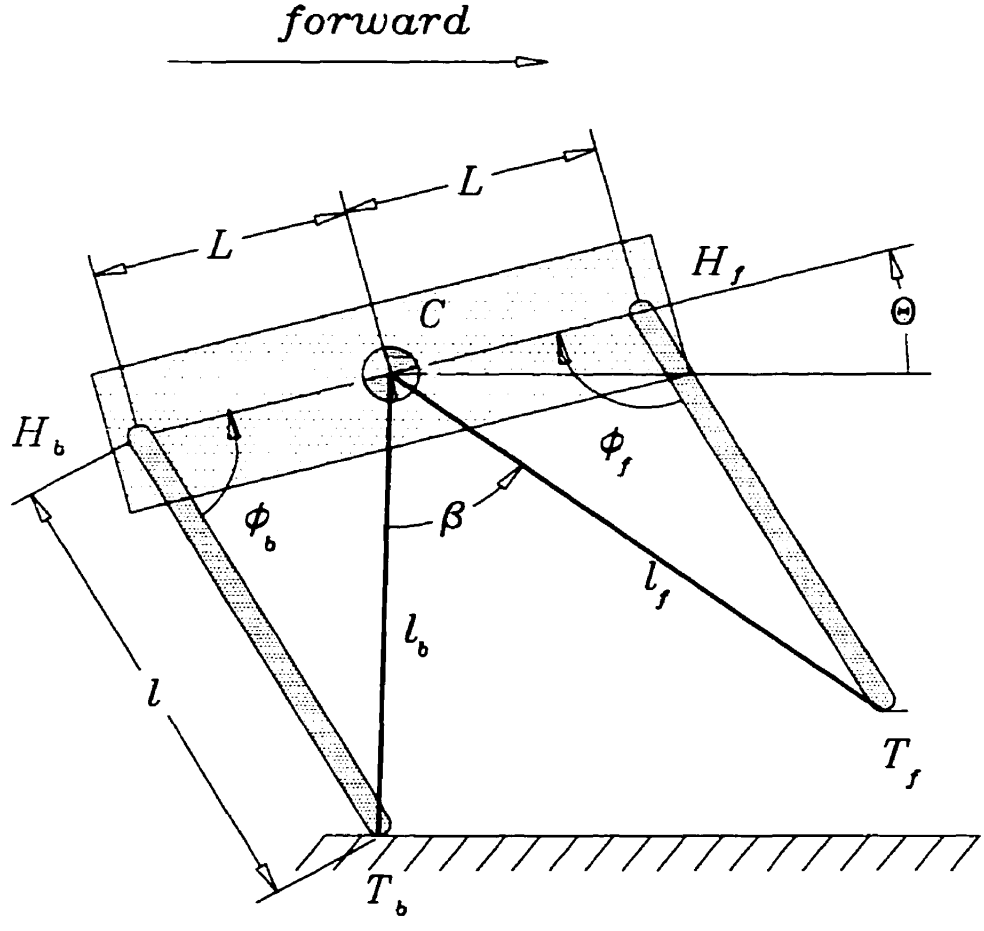


FIGURE 2.1. SCOUT model

hip angle ($\phi_b$, $\phi_f$). As a consequence, the length of the virtual leg is controlled via the hip actuators.

Given that SCOUT is a planar robot with stiff legs, it can perform only dynamic walking; that is, at any given instant, SCOUT is statically unstable. This implies that SCOUT is standing either on the front leg or the back leg. With this assumption, we ruled out the possibility of SCOUT being in a double support phase. Therefore, SCOUT can be modeled

- as an inverted double pendulum: the first link is the stance leg, and the second link is the body;

- as a variable length pendulum: the pendulum is the supporting virtual leg of variable length $l_{b,f}$.

It is important to note that, due to the assumption of massless legs, only the supporting leg influences the dynamics of the system. Both models, inverted double pendulum or variable length pendulum, are two DOF systems with only one actuator (the motor acting at the hip joint); therefore, it is an under-actuated system.

In Section 2.2 the equations that govern the motion while on either back leg support or front leg support will be presented. The mathematical model that governs the exchange of support will be introduced in Section 2.3. Tables 2.1 and 2.2 show the notation that will be used in the following sections and chapters.

| | |
|---|---|
| $l$ | leg length |
| $L$ | half the distance between hip joints |
| $m$ | body mass |
| $I$ | body moment of inertia about the center of mass |
| $r$ | body radius of gyration ($I = mr^2$) |
| $\theta$ | body angle w.r.t. the horizontal |
| $\phi_x$ | hip angle between body and leg |
| $l_x$ | virtual leg length |
| $\tau_x$ | torque applied by the hip actuator |

TABLE 2.1. Notation for SCOUT variables

| | |
|---|---|
| $X_b$ | support on back leg |
| $X_f$ | support on front leg |
| $X_{b,f}$ | support on either back or front leg |
| $X_n$ | n-th step |
| $X^B$ | value at back leg impact |
| $X^F$ | value at front leg impact |
| $X^{B-}$ | value just before back leg impact |
| $X^{F-}$ | value just before front leg impact |
| $X^{B+}$ | value just after back leg impact |
| $X^{F+}$ | value just after front leg impact |
| $X^*$ | desired value |

TABLE 2.2. Subscripts and superscripts used with SCOUT variables

## 2.2. Equations of Motion

In this section the equations of motion (EOM) describing SCOUT's single stance behavior will be presented; the inverted double pendulum model is considered in developing these equations. Different state variables describe the dynamics of the system while on back leg support or front leg support. Consequently, two different sets of EOM will be derived: however, a simple coordinate transformation between the states used in back leg support and front leg support will make the equivalence between the two sets of equations. The derivation of the EOM was done using the Lagrange Method.

In both back leg support and front leg support it is expected to derive a set of non-linear EOM. For some control analysis purposes the linearized version of these EOM might be of interest. The non-linear EOM describe accurately the motion of the system at any given configuration; however, the linear model approximates the dynamics of the system as long as the variables are close to the values specified in the linearization point.

**2.2.1. Back leg Support.** The non-linear EOM describing the dynamics of the system while on back leg support are given by,

$$\begin{cases} [r^2 + L^2 + l^2 - 2Ll\cos\phi_b]\ddot{\theta} - l[l - L\cos\phi_b]\ddot{\phi}_b \\ \qquad +2lL\dot{\phi}_b\dot{\theta}\sin\phi_b - Ll\dot{\phi}_b^2\sin\phi_b - gl\cos(\theta - \phi_b) + gL\cos\theta = 0 \\ -l[l - L\cos\phi_b]\ddot{\theta} + l^2\ddot{\phi}_b - lL\dot{\theta}^2\sin\phi_b + gl\cos(\theta - \phi_b) = \tau_b/m, \end{cases} \tag{2.1}$$

with the back hip torque $\tau_b$ being the input. In developing these equations we chose as state variables the body angle $\theta$ and hip angle $\phi_b$. The derivation of these equations is presented in Appendix A. Even though for controller development we assume the input to be the hip angle, for purposes of simulation we need a torque input model. A high gain PD controller will track the desired reference trajectory in $\phi_b$.

Eq. (2.1) was used in developing a numerical simulation in MATLAB [**6**]. For verification, the results of this simulation were compared with the results obtained

from a MOBILE simulation. In the MOBILE simulation the user specifies only the kinematic chain and mass, inertia properties describing the system under analysis, but not the EOM. This comparison, presented in Figure 2.2, validates the derived EOM.

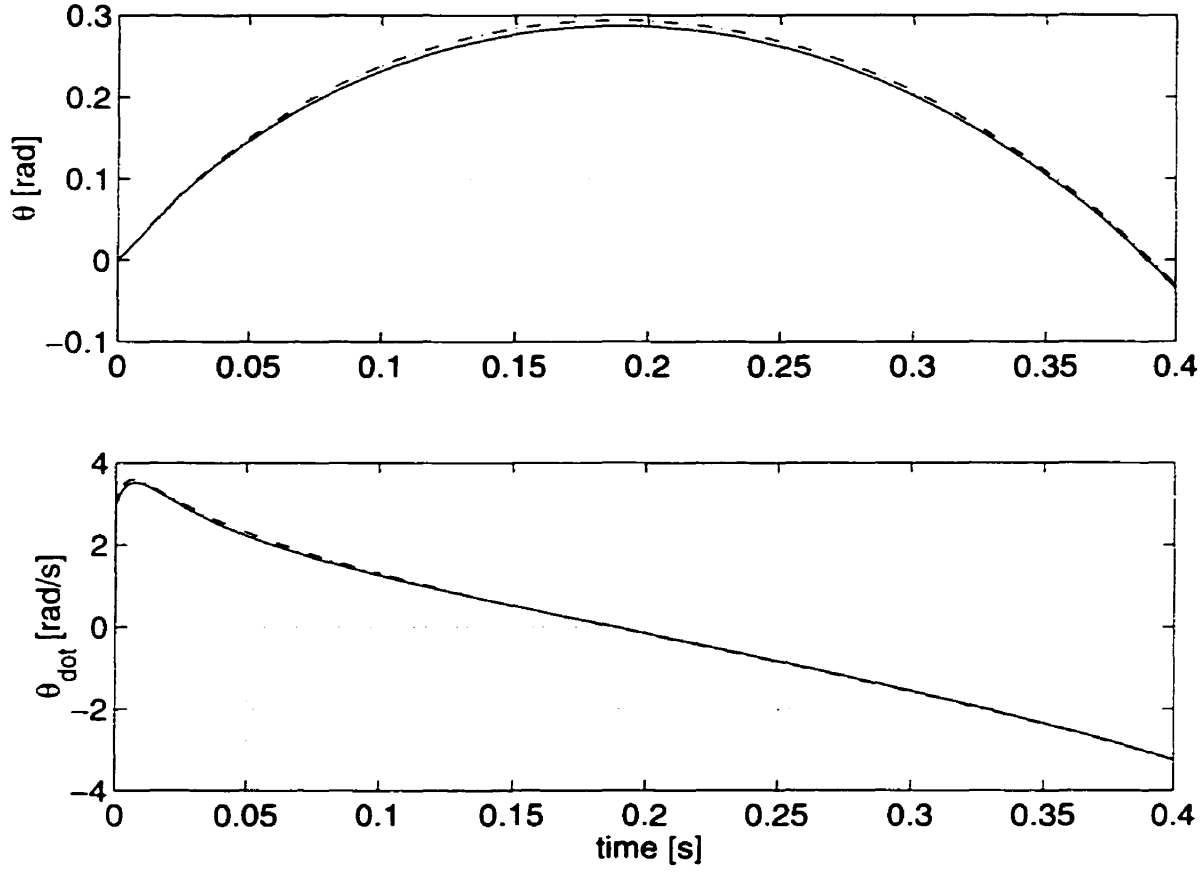


FIGURE 2.2. Body angle ($\theta$) obtained from MOBILE simulation (dashed line) and from the MATLAB simulation (solid line)

The linearized model of the system is often needed for control analysis purposes. During walking the body will have an oscillatory motion around $\theta = 0\ rad$; the leg will move around $\phi_b = \pi/2\ rad$ configuration and, given the future developed algorithms, with a constant angular velocity $\dot{\phi}_b = \dot{\phi}_{b,i}$. As a consequence, we linearized the EOM around

$$\theta = 0,\ \dot{\theta} = 0,\ \phi_b = \pi/2,\ \dot{\phi}_b = \dot{\phi}_{b,i}$$

to obtain

$$\begin{cases} l[r^2+L^2]\ddot{\theta}+2Ll^2\dot{\phi}_{b,i}\dot{\theta}-gL^2[\phi_b-\pi/2]-2Ll^2\dot{\phi}_{b,i}[\dot{\phi}_b-\dot{\phi}_{b,i}] \\ \qquad\qquad -l[\tau_b/m-gL]-Ll^2\dot{\phi}_{b,i}^2=0 \\ l[r^2+L^2]\ddot{\phi}_b+2Ll^2\dot{\phi}_{b,i}\dot{\theta}-g[2L^2+r^2][\phi_b-\pi/2]-2Ll^2\dot{\phi}_{b,i}[\dot{\phi}_b-\dot{\phi}_{b,i}] \\ \quad +g[r^2+L^2]\theta-[r^2+L^2+l^2][\tau_b/m-gL]/l-Ll^2\dot{\phi}_{b,i}^2-gL[r^2+L^2]/l=0. \end{cases} \tag{2.2}$$

The validity of these linear EOM was investigated, and Figure 2.3 shows a comparison between the body angle $\theta$ and body angular velocity $\dot{\theta}$ resulting from the integration of the linear (dashed line) and non-linear (solid line) EOM, for a constant back leg hip angular velocity $\dot{\phi}_{b,i}=2\ rad/s$. The results presented in Figure 2.3 were obtained from a MATLAB simulation (using the adaptive step size ODE45 integrator).

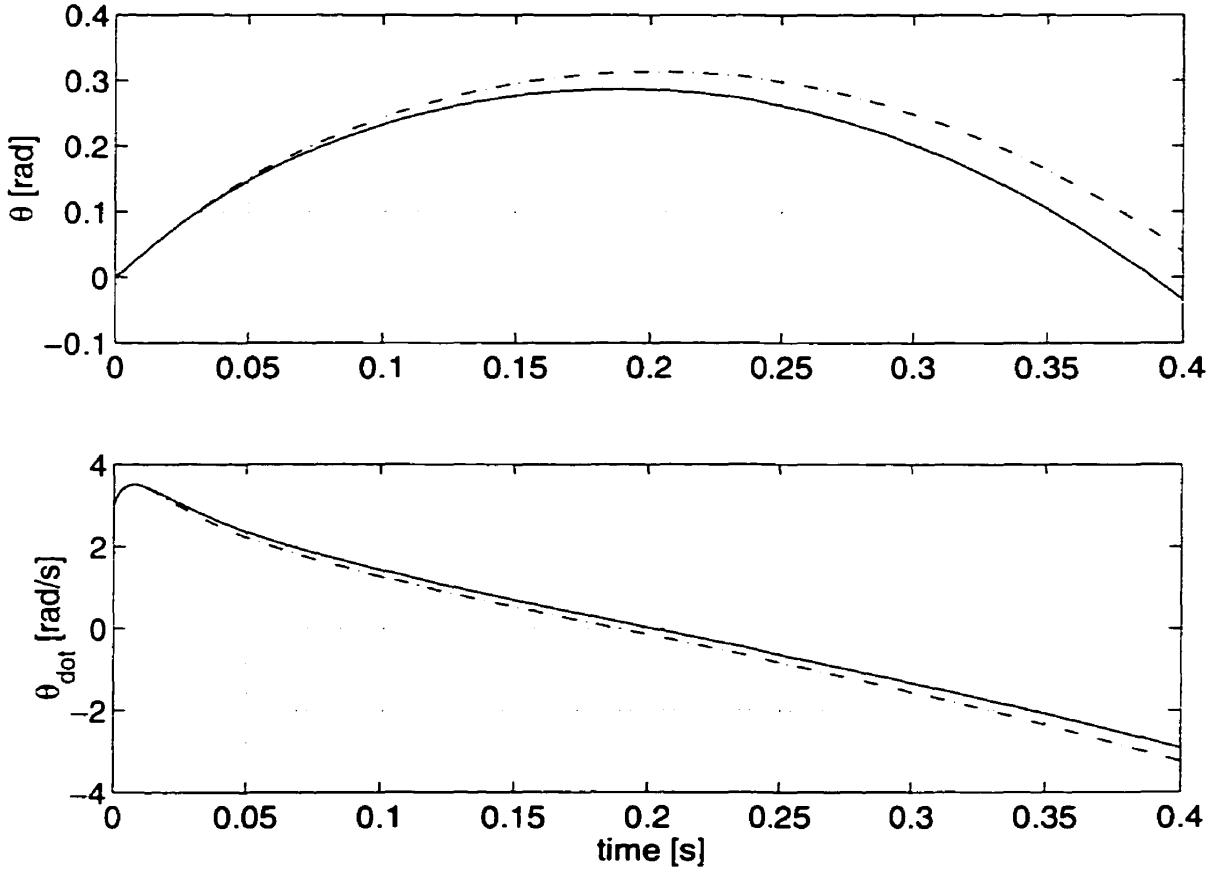


FIGURE 2.3. Comparison between the linear (dashed line) and non-linear (solid line) back leg support model

**2.2.2. Front leg Support.** The non-linear EOM while on front leg support are

$$\begin{cases} [r^2 + L^2 + l^2 - 2Ll\cos\phi_f]\ddot{\theta} + l[l - L\cos\phi_f]\ddot{\phi}_f + 2lL\dot{\phi}_f\dot{\theta}\sin\phi_f + Ll\dot{\phi}_f^2\sin\phi_f \\ \qquad\qquad +gl\cos(\theta+\phi_f) - gL\cos\theta = 0 \\ l[l - L\cos\phi_f]\ddot{\theta} + l^2\ddot{\phi}_f - lL\dot{\theta}^2\sin\phi_f + gl\cos(\theta+\phi_f) = \tau_f/m. \end{cases} \tag{2.3}$$

Again, the state variables are the body angle $\theta$ and the front leg hip angle $\phi_f$. These equations can be obtained from eq. (2.1) by the coordinate transformation

$$\begin{cases} \theta & \longrightarrow & \theta - \pi \\ \phi_b & \longrightarrow & 2\pi - \phi_f. \end{cases}$$

With the same considerations as presented in the Section 2.2.1, the linearization point was set as

$$\theta = 0,\ \dot{\theta} = 0,\ \phi_f = \pi/2,\ \dot{\phi}_f = \dot{\phi}_{f,i},$$

to obtain the linearized EOM

$$\begin{cases} l[r^2 + L^2]\ddot{\theta} + 2Ll^2\dot{\phi}_{f,i}\dot{\theta} - gL^2[\phi_f - \pi/2] + 2Ll^2\dot{\phi}_{f,i}[\dot{\phi}_f - \dot{\phi}_{f,i}] \\ \qquad\qquad +l[\tau_f/m - gL] + Ll^2\dot{\phi}_{f,i}^2 = 0 \\ l[r^2 + L^2]\ddot{\phi}_f - 2Ll^2\dot{\phi}_{f,i}\dot{\theta} - gr^2[\phi_f - \pi/2] - 2Ll^2\dot{\phi}_{f,i}[\dot{\phi}_f - \dot{\phi}_{f,i}] \\ \qquad -g[r^2 + L^2]\theta - [r^2 + L^2 + l^2][\tau_f/m - gL]/l - Ll^2\dot{\phi}_{f,i}^2 - gL[r^2 + L^2]/l = 0. \end{cases} \tag{2.4}$$

The detailed derivation of the linear and non-linear EOM is given in Appendix A. A MATLAB simulation was used to compare the results given by the linear and non-linear models. The body angle $\theta$ and angular velocity $\dot{\theta}$ resulting from linear (eq.

(2.4)) and non-linear (eq. (2.3)) model, for a constant front leg hip angular velocity $o_{f,i} = 2\ rad/s$, are presented in Figure 2.4.

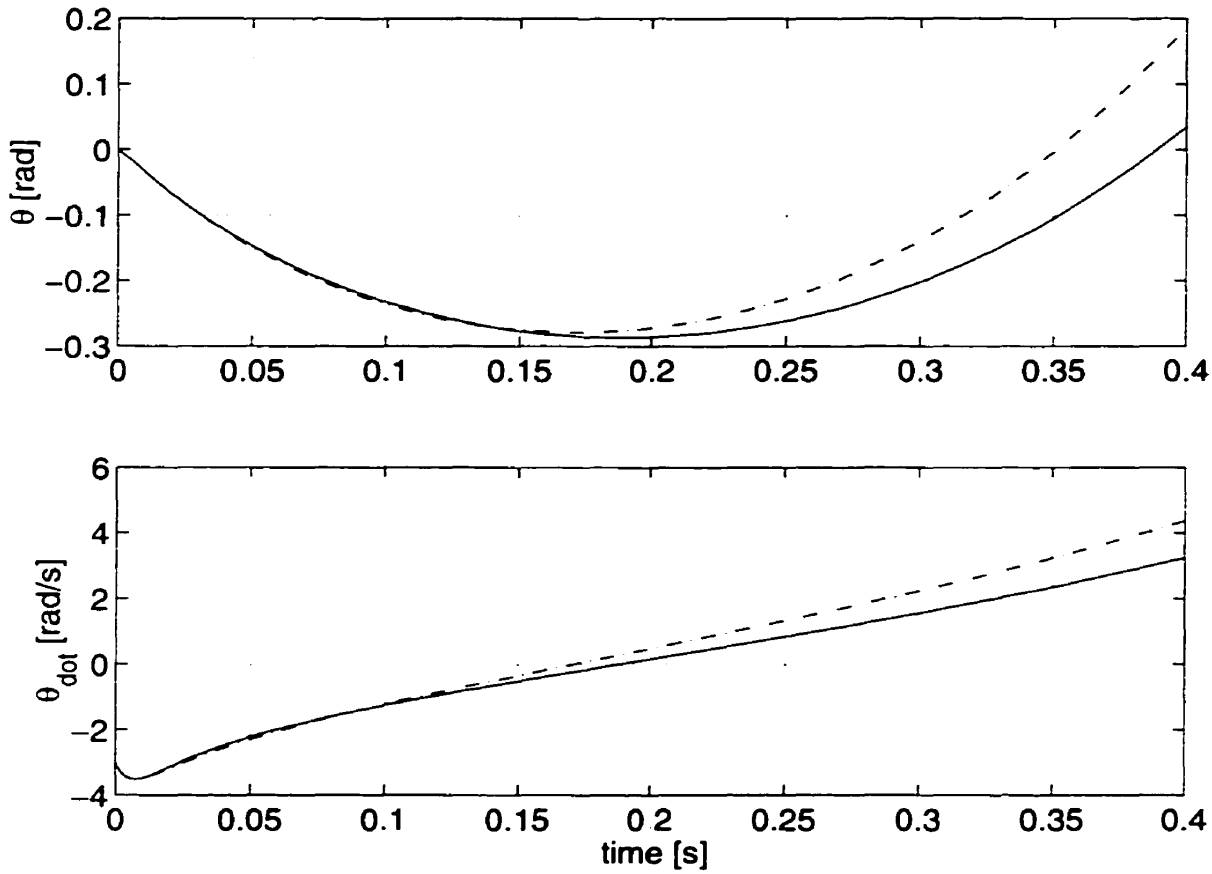


FIGURE 2.4. Comparison between the linear (dashed line) and non-linear (solid line) front leg support model

## 2.3. Impact Model

According to [**14**] for a system of interconnected bodies, under planar motion, for a finite time interval, $\Delta T$, the change of angular momentum of the system, $\Delta H_O$, is given by

$$\int_t^{t+\Delta T} \sum M_O dt = (\Delta H_O)_{system}. \tag{2.5}$$

where O is a fixed reference point and $H_O$ the angular momentum. The moment summation includes only the effect of external forces (equal and opposite actions and reactions at the interconnections are internal to the system and cancel one another). Using the above definition we can determine the change in the angular momentum at the exchange of the supporting leg (impact of the free leg). During the impact the only external force comes from gravity, but the impact time is very short, that is $\Delta T$ approaches zero, and therefore the angular momentum of the system with respect to the impacting toe is conserved,

$$(\Delta H_O)_{system} = 0. \tag{2.6}$$

This result was used also by McGeer [**11, 13, 12**] in his analysis of the rimless wheel and gravity powered wheel, and by Dunn and Howe [**4, 5**] in their analysis of bipedal walking.

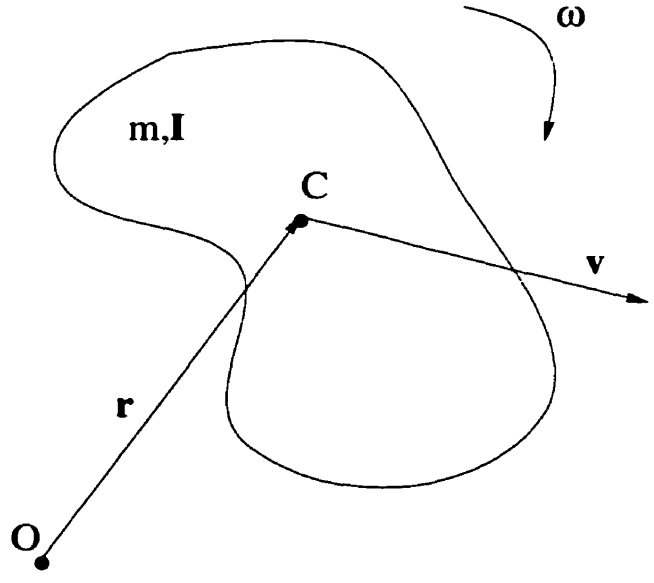


FIGURE 2.5. Angular momentum of a body w.r.t a point

The angular momentum of of a body about any point $O$ (Figure 2.5) is given by

$$\mathbf{H_O} = \mathbf{I}\omega + \mathbf{r} \times m\mathbf{v} \ ,$$

where $\mathbf{H_O}$ is the vector of angular momentum about point O, $\mathbf{I}$ is the body inertia matrix about the centre of mass, $\omega$ is the vector of body absolute angular velocity, $\mathbf{r}$ is the position vector from the leg toe to the body center of mass, $m$ is the body mass, and $\mathbf{v}$ is the center of mass velocity vector.

Since SCOUT is assumed to have planar motion we are only interested in the angular momentum about the axis perpendicular to the plane. We can also express the moment of inertia about this axis as the product between the mass and square of the radius of gyration; hence, from the above vectorial expression we can extract the $z$ component to obtain

$$H_{T_z} = mr^2\dot{\theta} + m(\mathbf{r}_{T_zC} \times \mathbf{v}_C)_z \ , \tag{2.7}$$

where $H_{T_z}$ is the z component of the angular momentum with respect to back leg $T_b$ or front leg toe $T_f$ (see Figure 2.1), $\mathbf{r}_{T_zC}$ is the position vector from the impacting toe ($T_b$ or $T_f$) to the center of mass ($C$) , and $\mathbf{v}_C$ is the center of mass velocity vector.

The conservation of angular momentum during impact will allow us to determine the after-impact state for the system. As in the case of the derivation of the EOM, where we distinguished between the back leg and front leg support cases, two sets of equations must be derived in terms of the supporting leg. In both cases we start with conservation of angular momentum (eq. (2.6)),

$$H^- = H^+$$

where $H^-$ and $H^+$ are the angular momentum just before and immediately after impact.

The following two sections will present the model describing the front leg and back leg impact. Subsection 2.3.1 presents the impact model based on the states used in

double pendulum model (body angle $\theta$ and supporting leg hip angle $\phi_b$ or $\phi_f$). Subsection 2.3.2 considers the states used in the variable length pendulum model (body angle $\theta$ and length of supporting virtual leg $l_b$ or $l_f$). The impact models presented in Subsection 2.3.2 are equivalent, through simple coordinate transformations, to the models presented in Subsection 2.3.1. The detailed derivations of the momentum transfer equations are presented in Appendix B.

**2.3.1. Impact Model Based on the Double Pendulum Model.** From eqs. (2.7) and (2.6), and conservation of angular momentum when the back leg impacts gives

$$\begin{aligned}
&\left[l[-l\cos(\phi_b^B+\phi_f^B)+L\cos\phi_f^B]+r^2-L^2+lL\cos\phi_b^B\right]\dot{\theta}^{B-}\\
&\qquad +l[-l\cos(\phi_b^B+\phi_f^B)+L\cos\phi_f^B]\dot{\phi_f}^{B-}\\
&=\left[l[l-L\cos\phi_b^B]+r^2+L^2-lL\cos\phi_b^B\right]\dot{\theta}^{B+}-l[l-L\cos\phi_b^B]\dot{\phi}_b^{B+}. \qquad (2.8)
\end{aligned}$$

The known variables are the ones that define the configuration at back leg impact (hip angles $\phi_b^B, \phi_f^B$) and the before-impact angular velocities $\dot{\theta}^{B-}$, $\dot{\phi}_f^{B-}$. The change of support is very short; therefore, we assume that the configuration of the system remains the same and that only the velocities undergo step changes in their values. The unknown values are the after-impact angular velocities of the body and the impacting leg's hip ($\dot{\theta}^{B+}$ and $\dot{\phi}_b^{B+}$).

A second equation can be determined from the conservation of angular momentum about the impacting leg hip. For simplicity of the control scheme, we make the additional assumption that it is possible to control the angular velocity of the impacting hip ($\dot{\phi}_b^{B+}$) during the support exchange. With this assumption, eq. (2.8) can be used to determine the after-impact angular velocity of the body $\dot{\theta}^{B+}$.

In order to check the validity of the above momentum transfer equation, we used another simulation package, WORKING MODEL. This package does not use an algebraic calculation for the after impact velocities as in eq. (2.8), but rather integrates all moments over a finite period of time, as in eq. (2.5). Starting from

| | | | | |
|---|---|---|---|---|
| $\dot{\theta}^{B+}[rad/s]$ (eq. (2.8)) | -0.57 | -0.74 | -0.83 | -0.63 |
| $\dot{\theta}^{B+}[rad/s]$ (WORKING MODEL) | -0.56 | -0.73 | -0.82 | -0.61 |
| Error [%] | 0.85 | 1.32 | 1.50 | 2.58 |

TABLE 2.3. Validation of momentum transfer equation

a given before-impact states $(\dot{\theta}^{B-}, \dot{\phi}_f^{B-}, \phi_b^B, \phi_f^B)$. Table 2.3 contains in its first row the theoretical obtained value (eq. (2.8)) and on the second row the value resulting from the WORKING MODEL simulation. The impact model used in WORKING MODEL can explain the errors indicated in the last row. In developing eq. (2.8), it was assumed that the impact between the leg and ground is perfectly plastic and just after the impact the connection between the leg and ground can be modeled as a free pin join. In WORKING MODEL a more realistic model is used, namely the connection between the leg and ground, produced after the impact, is a result of the friction properties of both leg and ground materials. Given these differences, the small errors obtained confirm the validity of the momentum transfer eq. (2.8).

Eq. (2.9) expresses the conservation of angular momentum when the front leg impacts,

$$\begin{aligned} &\left[l[-l\cos(\phi_b^F+\phi_f^F)+L\cos\phi_b^F]+r^2-L^2+lL\cos\phi_f^F\right]\dot{\theta}^{F-} \\ &\qquad -l[-l\cos(\phi_b^F+\phi_f^F)+L\cos\phi_b^F]\dot{\phi}_b^{F-} \\ &= \left[l[l-L\cos\phi_f^F]+r^2+L^2-lL\cos\phi_f^F\right]\dot{\theta}^{F+}+l[l-L\cos\phi_f^F]\dot{\phi}_f^{F+}. \end{aligned} \tag{2.9}$$

Detailed derivations of eqs. (2.8) and (2.9) are given in Appendix B.

**2.3.2. Impact Model based on the Virtual Leg Model.** The polynomial controller (Section 3.2) will use the variable length pendulum system model. In this model the variables defining the degrees of freedom are the body angle $\theta$ and the length of the supporting virtual leg $l_x$. This section will present the mathematical model describing the impact of the virtual back leg and virtual front leg.

Referring to eq. (2.7), the conservation of angular momentum when the virtual back leg impacts with the ground is given by

$$[r^2 + l_b^B l_f^B \cos\beta^B]\dot{\theta}^{B-} + [l_b^B \sin\beta^B - C_f^B l_b^B l_f^B \cos\beta^B]\dot{l_f}^{B-} = [r^2 + (l_b^B)^2]\dot{\theta}^{B+} - C_b^B (l_b^B)^2 \dot{l_b}^{B+}. \quad (2.10)$$

where $C_b^B$, $C_f^B$ are constants depending only on SCOUT's dimensions (body length and leg length) and on the configuration at back leg impact ($l_b^B$, $l_f^B$). Their explicit form is given in Appendix B.

The same principle of conservation of angular momentum is used in deriving the mathematical model (eq. (2.10)) governing the impact of the front virtual leg,

$$[r^2 + l_b^F l_f^F \cos\beta^F]\dot{\theta}^{F-} - [l_f^F \sin\beta^F + C_b^F l_b^F l_f^F \cos\beta^F]\dot{l_b}^{F-} = [r^2 + (l_f^F)^2]\dot{\theta}^{F+} - C_f^F (l_f^F)^2 \dot{l_f}^{F+}. \quad (2.11)$$

The constants $C_b^F$, $C_f^F$ are, again, depending on SCOUT's dimensions and configuration at impact.

# CHAPTER 3

# WALKING CONTROL ALGORITHMS

## 3.1. Problem Formulation

As introduced in Section 2.1, SCOUT can be modeled as two 2-DOF systems, one for back leg stance and one for front leg stance. The single actuator per model is placed at the hip joint (either $H_b$ or $H_f$ in Figure 2.1). For purposes of controller design we assume that we can control directly and instantaneously the hip angles and angular velocities; thus, our inputs are $\phi_f(t)$ and $\phi_b(t)$. However, the simulations (and, of course, the experiments) used a PD controller to determine the hip torque necessary to track the hip angle desired trajectory. The states of interest to be controlled are the body angle and angular velocity

$$\Theta = \begin{bmatrix} \theta \\ \dot{\theta} \end{bmatrix}.$$

One complete step consists of two leg support phases, one for each leg, and two impacts, as illustrated by the block diagram in Figure 3.1. For purposes of analysis it

is convenient to examine the variable of interest, $\Theta$, at only one instant in this step, and we chose the instant immediately following the back leg impact,

$$\Theta_n \triangleq \Theta^{B+} = \begin{bmatrix} \theta^B \\ \dot{\theta}^{B+} \end{bmatrix}. \tag{3.1}$$

Now we can define a discrete step-to-step return map, $\mathcal{S}$, which maps the body states just after impact from step $n$ to step $n+1$, as a function of the inputs $\phi_b(t), \phi_f(t)$,

$$\Theta_{n+1} = \mathcal{S}(\Theta_n, \phi_b(t), \phi_f(t)). \tag{3.2}$$

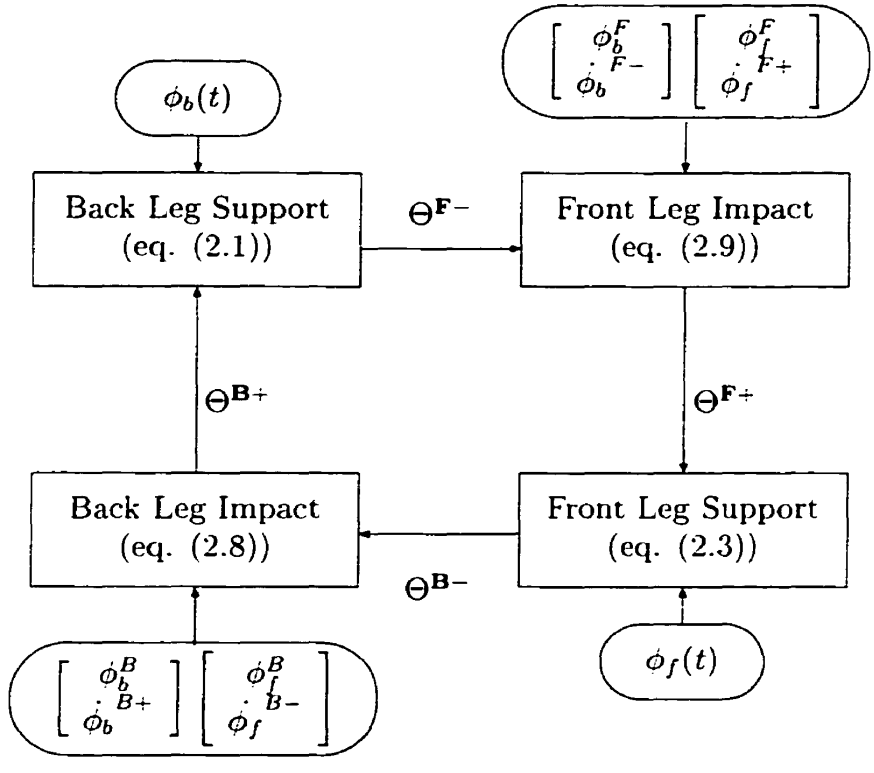


FIGURE 3.1. Control inputs during a complete step

For the polynomial controller (Section 3.2) and saturated ramp controller (Section 3.4) the controlled inputs already determine $\theta^B$, so eq. (3.2) becomes a scalar return map for $\dot{\theta}^{B+}$. The control objective can be stated as finding continuous hip angle trajectories, $\phi_b(t), \phi_f(t)$, which make the desired body states, $\Theta^*$, an asymptotically

stable fixed point of the return map $\mathcal{S}$. In the remainder of this section, we will present three such hip angle trajectories.

## 3.2. Polynomial Controller

The initial approach was to simplify the problem by analyzing the system formed by the virtual legs ($l_b$, $l_f$ in Figure 2.1). As a result, the system that needs to be analyzed is a biped with variable leg length. Our control algorithm is based on the idea of imposing a certain after-impact angular velocity for the body $\dot{\theta}^{B+}$ and $\dot{\theta}^{F+}$. Using the momentum transfer eqs. (2.11) and (2.10), from the desired after-impact angular velocity for the body $\dot{\theta}^{F+}$ (or $\dot{\theta}^{B+}$), and assuming that the impacting virtual leg has a constant length $\dot{l}_f^{F+} = 0$ (or $\dot{l}_b^{B+} = 0$), we can fully determine the RHS of the momentum transfer eq. (2.11) (or eq. (2.10)). On the LHS of the eq. we have two unknowns, the angular velocity of the body at touch down, $\dot{\theta}^{F-}$ (or $\dot{\theta}^{B-}$ ), and the time rate of change of the length of the supporting virtual leg, $\dot{l}_b^{F-}$ (or $\dot{l}_f^{B-}$ ) (we refer to $\dot{l}$ as being the *linear velocity* of the leg). Because we are analyzing an underactuated system, of the two variables $[\dot{\theta}^{F-}, \dot{l}_b^{F-}]$ (or $[\dot{\theta}^{B-}, \dot{l}_f^{B-}]$), we are able to control only the velocity of the virtual leg directly via the hip actuator. Therefore, the momentum transfer can be controlled through the velocity of the supporting leg at impact time, via

$$\dot{l}_b^{F-} = c_1\dot{\theta}^{F-} + c_2\dot{\theta}^{F+} \tag{3.3}$$

$$\dot{l}_f^{B-} = c_3\dot{\theta}^{B-} + c_4\dot{\theta}^{B+}, \tag{3.4}$$

where the $c_i$ are functions of the virtual leg lengths, and are given in detail in Appendix B. If, at front leg impact, $\dot{l}_b^{F-}$ has the value given in eq. (3.3), then using eq. (2.11), one can observe that $\dot{\theta}^{F+}$ will result in its desired set point value. The same observation is valid for the back leg impact, with $\dot{l}_f^{B-}$ given by eq. (3.4). Unfortunately, the body angular velocity just before the impact $\dot{\theta}^{F-}$ (or $\dot{\theta}^{B-}$) is not known a priori since it is coupled dynamically to the applied control input.

In order to solve this problem, we use an estimate of this value. That is, after each time step, we assume that from that moment on, until front or back leg impact, the virtual leg will have a constant length - therefore the system will behave like an inverted pendulum. Using the dynamics of an inverted pendulum, we predict the touchdown angular velocity, $\dot{\theta}^{B-}$ (or $\dot{\theta}^{F-}$), at each controller time step. On the other hand, we assume that we specify the kinematic configuration at impacts, via $l_b^B$, $l_f^F$, a priori, and assume those to be known.

With this, the supporting virtual leg length should satisfy four conditions: the initial length, final length, initial and final linear velocities. It was mentioned that the impacting leg will have constant length just after the impact, that is, $\dot{l}_f^{F+} = 0$ and $\dot{l}_b^{B+} = 0$. For simplicity, the actuation will start when the body reaches the apex. A third order polynomial in the absolute body angle that describes the variation of the virtual leg length suffices to meet all four conditions,

$$l_{b,f}(\theta) = a_3\theta^3 + a_2\theta^2 + a_1\theta + a_0. \tag{3.5}$$

The coefficients of the polynomial are determined from the initial and final conditions.

$$\begin{aligned}
l_b(\theta_{init}) &= a_3\theta_{init}^3 + a_2\theta_{init}^2 + a_1\theta_{init} + a_0 &&= l_{b_{init}} \\
l_b(\theta^F) &= a_3(\theta^F)^3 + a_2(\theta^F)^2 + a_1\theta^F + a_0 &&= l_b^F \\
\dot{l}_b(\theta_{init}) &= (3a_3\theta_{init}^2 + 2a_2\theta_{init} + a_1)\dot{\theta}_{init} &&= \dot{l}_{b_{init}} \\
\dot{l}_b(\theta^F) &= (3a_3(\theta^F)^2 + 2a_2\theta^F + a_1)\dot{\theta}^{F-} &&= \dot{l}^{F-}.
\end{aligned} \tag{3.6}$$

The equations form a linear system in the unknown coefficients of the polynomial. For simplicity we presented only the conditions imposed on the back virtual leg, but similar expressions can be written for the front virtual leg. Given that the final angular velocity of the body, $\dot{\theta}^{F-}$ ($\dot{\theta}^{B-}$), is predicted continuously, this system will have to be solved, for the polynomial coefficients, after each prediction. The initial conditions ($\theta_{init}, \dot{\theta}_{init}, l_{b_{init}}, \dot{l}_{b_{init}}$) are set as their current values. The final conditions

$\theta^F$ ($\theta^B$), $l_b^F$ ($l_f^B$) are determined by the configuration at impacts and $\dot{l}_b^{F-}$ ($\dot{l}_f^{B-}$) is re-computed from eq. (3.4) (or (3.3)) according to the new $\dot{\theta}^{F-}$ ($\dot{\theta}^{B-}$) prediction.

In order to implement this algorithm, we need to specify information beyond the body states just after back leg impact, $\Theta^{B+}$, which is used for purposes of analysis in the return map. In particular, we need to specify the configurations at exchange of support ($[\phi_b^B, \phi_f^B]$, $[\phi_b^F, \phi_f^F]$) and desired after-impact body angular velocities ($\dot{\theta}^{F+}, \dot{\theta}^{B+}$). The possible combinations of these parameters are limited by the solutions for the system of linear eqs. (3.6). Furthermore, the $\dot{\theta}^{B+}$, $\dot{\theta}^{F+}$ values are limited by the turn over. We selected the following set points.

$$\begin{cases} \phi_b^F = 1.71 \ rad \\ \phi_f^F = 1.53 \ rad \\ \dot{\theta}^{F+} = -1.00 \ rad/s \\ \phi_b^B = 1.43 \ rad \\ \phi_f^B = 1.53 \ rad \\ \dot{\theta}^{B+} = 1.00 \ rad/s. \end{cases}$$

The particular choice for the configuration at impacts was motivated by hardware limitations on SCOUT (maximum available torque from the hip actuators). The $\dot{\theta}^{B+}$, $\dot{\theta}^{F+}$ set point values resulted from a set of MOBILE simulations. These values are large enough to prevent premature touchdown of the flight leg, and small enough to prevent turn over.

The results of a MOBILE simulation are shown in Figure 3.2. The top and middle graphs present the body angle $\theta$ and body angular velocity $\dot{\theta}$ variation during the simulated walking motion. The bottom graph presents the variation, according to eq. (3.5), of the supporting hip angle $\phi_{b,f}$. The dashed lines show exchange of support (the motion starts when the back leg is in stance). The simulation started from an arbitrary initial configuration; as shown in the the top graph, this configuration was away from the desired steady state motion. However, Figure 3.2 shows that just one step is sufficient to recover from this initial error.

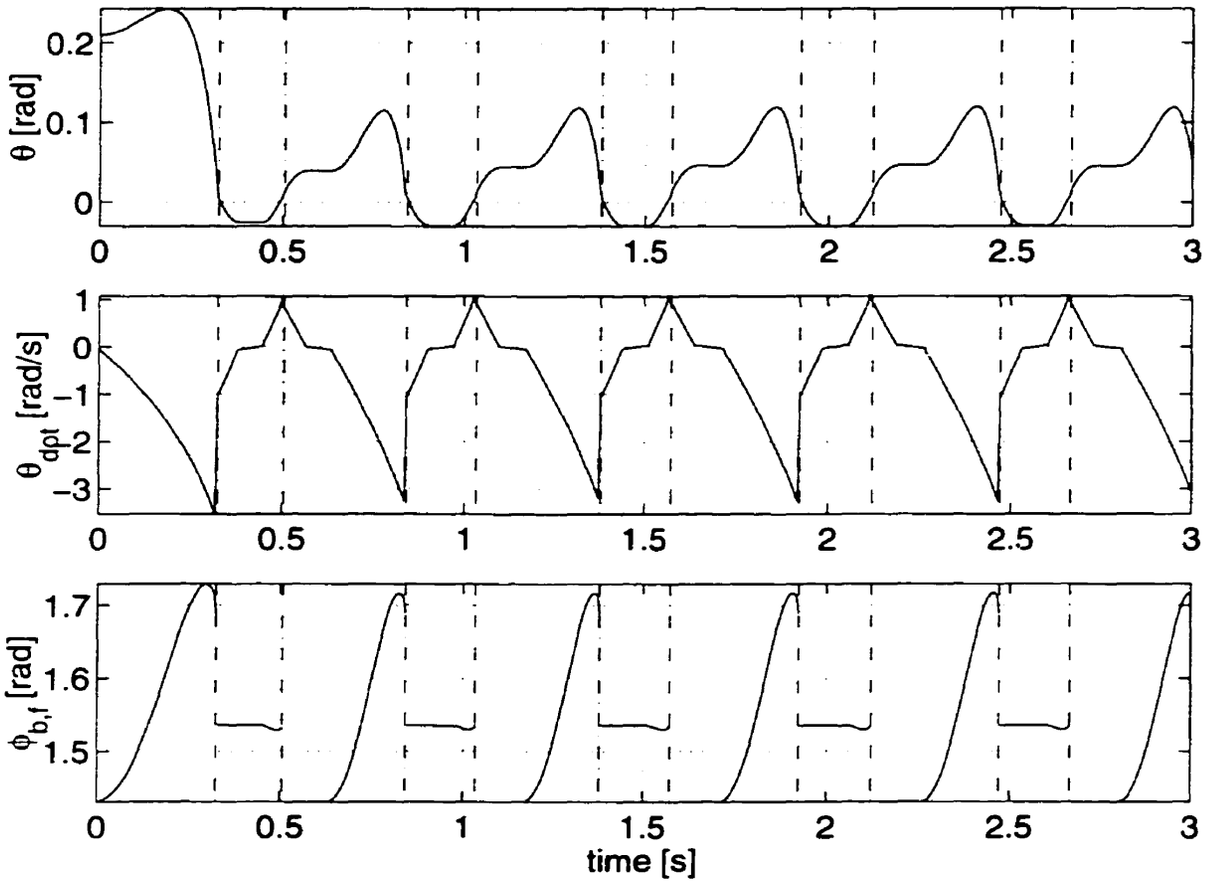


FIGURE 3.2. Polynomial controller with continuous update of $\dot{\theta}^{B-}$, $\dot{\theta}^{F-}$

We are interested in control strategies which are robust and can be implemented with minimal sensing. So far the control scheme requires that the stance virtual leg remains at a constant length until the body reaches its apex (maximum body angle). At that instant, a polynomial for the supporting virtual leg length is planned according to eq. (3.5). The polynomial coefficients calculations require the prediction of the before-impact angular velocity. A further simplification is introduced, namely the prediction of the touch down body angular velocity, which is done only once at apex. When the single prediction of $\dot{\theta}^{B-}$ ( $\dot{\theta}^{F-}$) is adopted, a fixed, second order polynomial for the length of the supporting virtual leg is sufficient. This is a major simplification, but, as shown in Figure 3.3, results in a periodic motion with performances close to the desired set points of $\dot{\theta}^{B+} = 1.0\ rad/s$, $\dot{\theta}^{F+} = -1.0\ rad/s$.

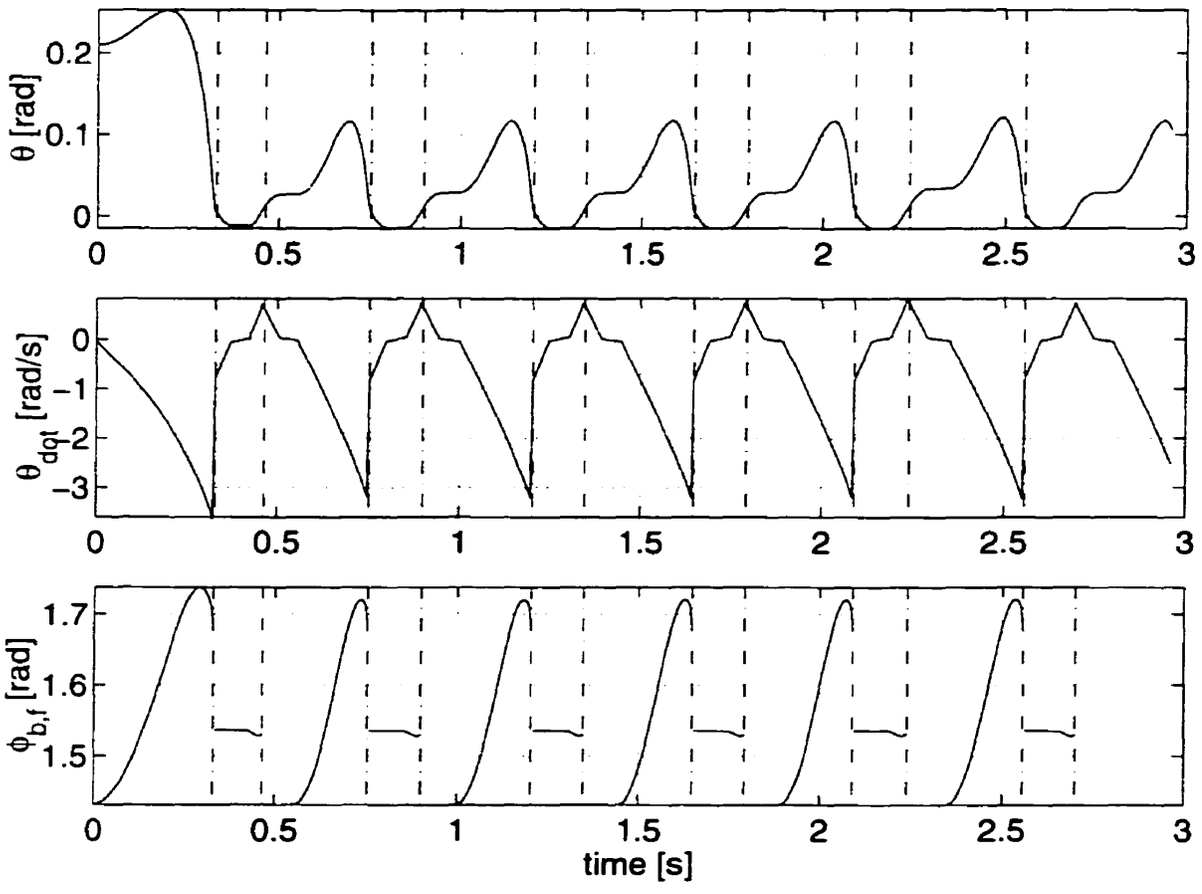


FIGURE 3.3. Polynomial controller with no update

The differences between using a third order polynomial (hence continuous update of $\dot{\theta}^{B-}$ or $\dot{\theta}^{F-}$) and a fixed, second order polynomial are evident in the resulting after-impact body angular velocities. Figure 3.4 shows the resulting $\dot{\theta}^{B+}$ from a large initial error using the third degree polynomial ('+') and the fixed, second order polynomial ('o'); the dashed line indicates the desired set point value. The one time estimation of the before-impact body angular velocity results in an error of less than 5%. This represents an acceptable error in practice. Furthermore, the reduced complexity of the controller recommends it for practical implementations. Figure 3.4 indicates that the steady state value obtained for the after-impact angular velocity $\dot{\theta}^{B+}$ is offseted from its desired value. To eliminate this offset, an integral term can be added in the

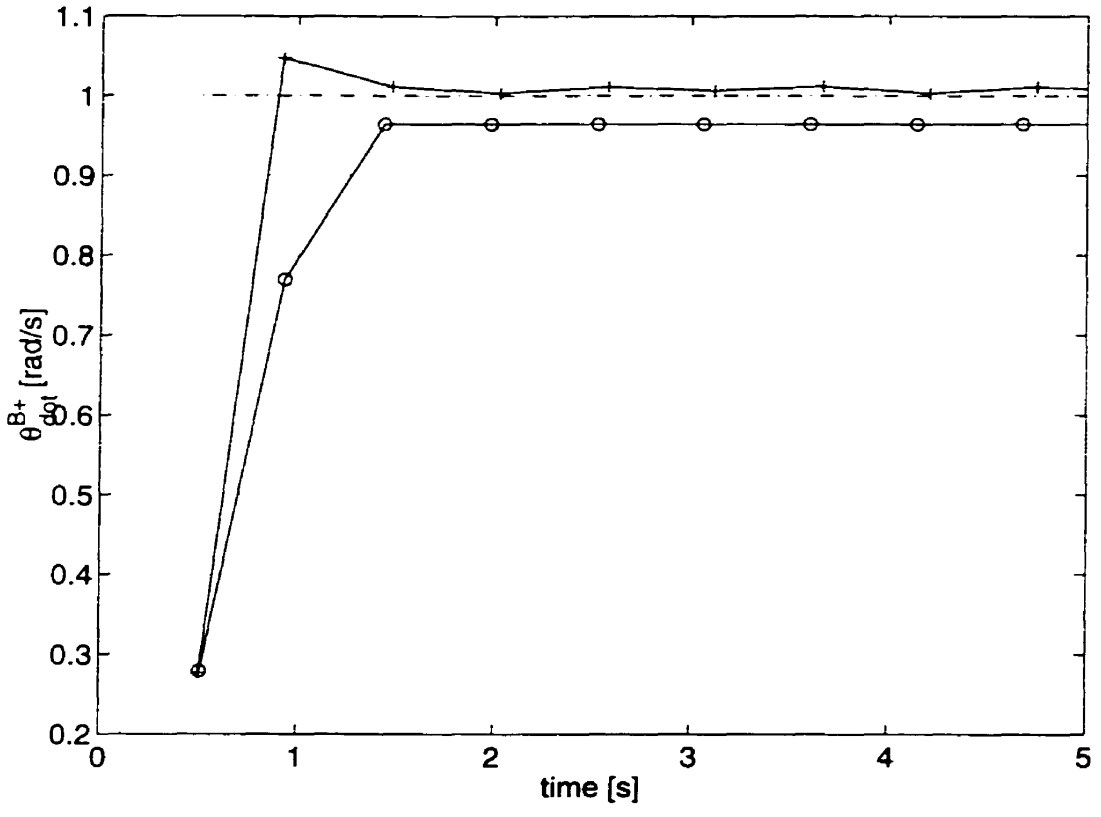


FIGURE 3.4. $\dot{\theta}^{B+}$ ('+') with update on polynomial coefficients and ('o') without update

control scheme, or a look-up table for compensation terms can be developed. This subject has not been pursued at this time.

A successful controller must still be able to compensate disturbances. If there is a sufficient range of permissible $\dot{l}_b^{F-}$ ($\dot{l}_f^{B-}$) around the nominal value, eqs. (3.3) and (3.4) can be utilized to eliminate errors online and to achieve the desired body angular velocities $\dot{\theta}^{F+}$ ($\dot{\theta}^{B+}$). Figure 3.5 shows the large range of disturbances in $\dot{\theta}^{B+}$ from which recovery is still possible, even when a fixed, second order polynomial is used. This range is limited by either turn over or toe stubbing. A simplified version of this control algorithm has been implemented on SCOUT I and resulted in stable walking [**2**].

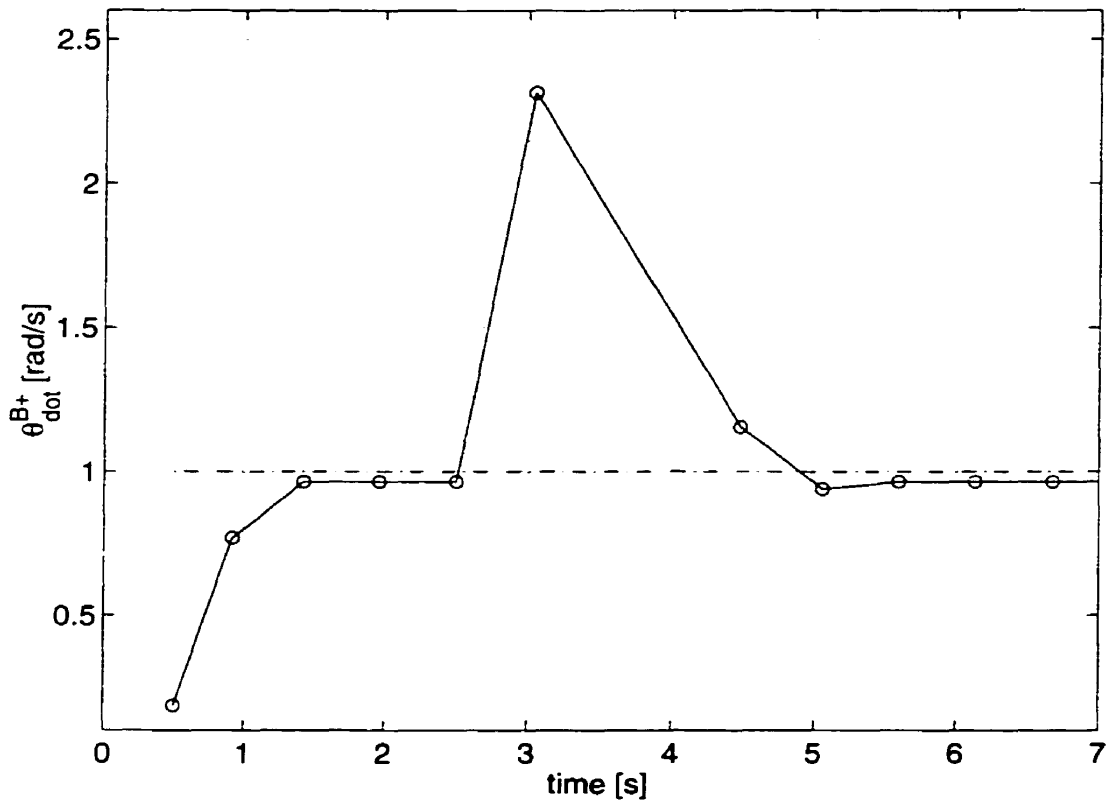


FIGURE 3.5. Recovery from severe disturbances using a fixed, second order polynomial

## 3.3. Ramp Controller

With the experience gained from the implementation of the controller presented in Section 3.2 on SCOUT I, we moved towards control algorithms that require simpler actuation functions which are easier to implement. In particular, we will show that a constant angular velocity for the back hip during back leg support and a fixed hip angle for the front leg will result in stable walking. During the back leg support phase we will prescribe a ramp function for $\phi_b(t)$ (Figure 3.6). The after-impact back leg hip angle $\phi_b^B$ and the slope of the ramp $\dot{\phi}_b$, will be design parameters. The parameters defining the ramp input, $[\phi_b^B,\ \dot{\phi}_b]$, will also determine the value of the back leg hip angle at front leg impact.

A set of MATLAB simulations was used to determine the influence of different parameters on the overall motion. These simulations integrated the inverted double

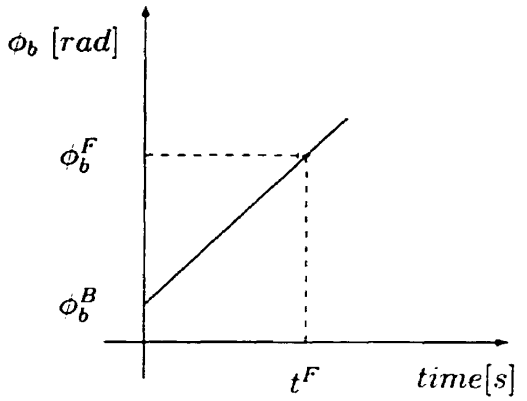


FIGURE 3.6. Ramp input for the back hip angle

pendulum mathematical model of the system for one step (Figure 3.1). For a certain constant angular velocity of the back hip actuator, we investigated the influence of the front leg orientation $\phi_f^F$ on the initial body angular velocity for the front leg support phase $\dot{\theta}^{F+}$. Figure 3.7(a) shows that, as the front leg angle increases, the resulting magnitude of $\dot{\theta}^{F+}$ decreases; for large $\phi_f^F$ values we expect $\dot{\theta}^{F+} > 0$, which means that the impact of the front leg will not result in a lift off of the back leg. Ideally we would like to have the magnitude of $\dot{\theta}^{F+}$ as large as possible. Consequently, the front leg should be positioned at a small angle. In the back leg support phase, the supporting leg sweeps from a small angle to a large one, giving a forward displacement for the center of mass. In the front leg support phase, a sweep of the supporting leg from a small value to a large value will induce an unwanted backwards displacement for the center of mass. For this reason, we decided to keep the front legs fixed at all times. Next, we investigated the optimal orientation of the front legs that will result in a periodic motion ($\dot{\theta}_{n+1}^{B+} = \dot{\theta}_n^{B+}$). Starting with $\dot{\theta}_n^{B+} = 1\ rad/s$ the results presented in Figure 3.7(b) show that the periodic motion condition is satisfied for a front leg orientation of $\phi_f = 1.31\ rad$. We also investigated the effect of the back hip actuator angular velocity on the next step initial body angular velocity. Figure 3.7(c) shows the possible $\dot{\theta}_{n+1}^{B+}$ for a span of possible $\dot{\phi}_b$ and $\dot{\theta}_n^{B+} = 1\ rad/s$. Again, considering the periodic motion condition, we chose $\dot{\phi}_b = 0.85\ rad/s$.

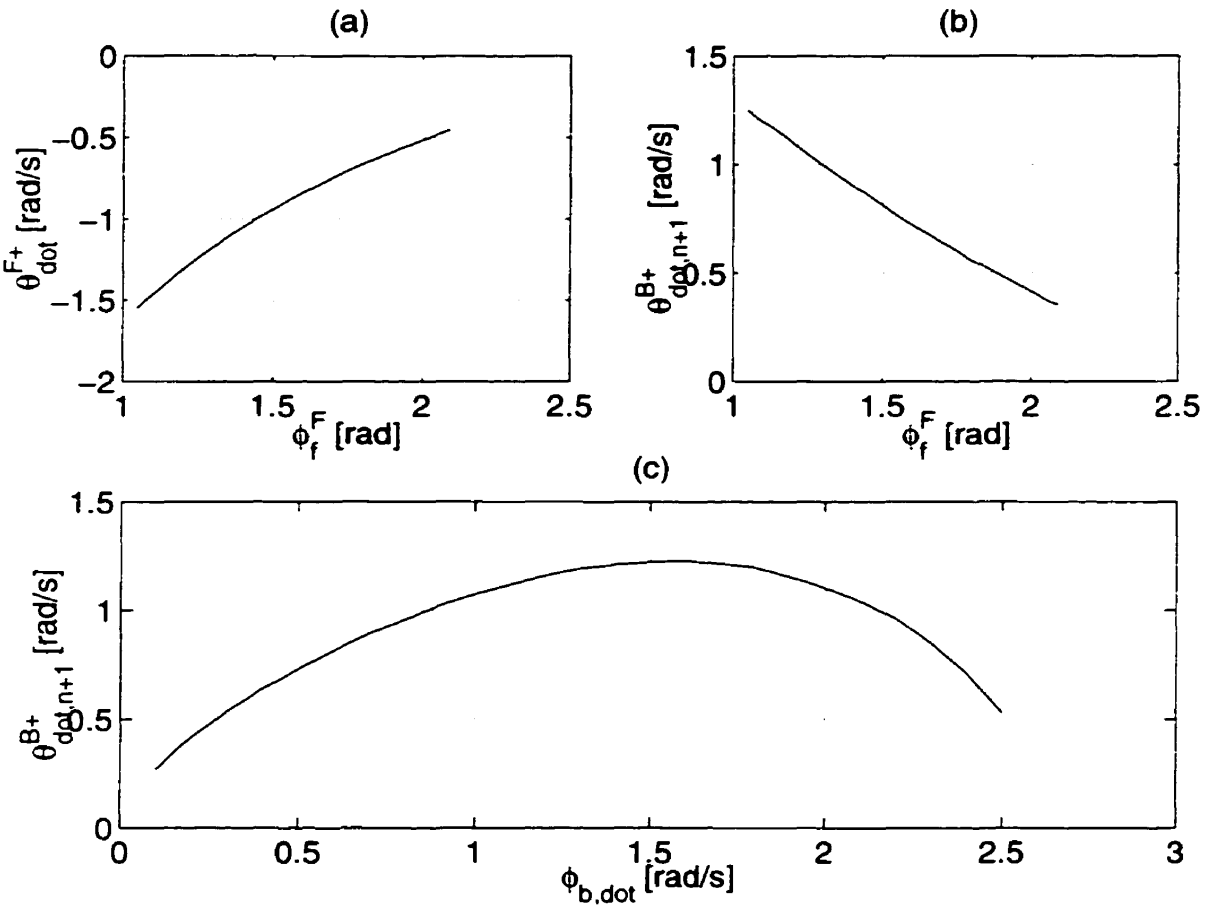


FIGURE 3.7. Effect of $\phi_f^F$ (a) on $\dot{\theta}^{F+}$ and on (b) $\dot{\theta}^{B+}_{n+1}$ : (c) effect of $\dot{\phi}_b$ on $\dot{\theta}^{B+}_{n+1}$

With all of these factors analyzed, a numerical simulation with

$$\begin{cases} \phi_b^B &= 1.05\ rad \\ \dot{\phi}_b &= 0.85\ rad/s \\ \phi_f &= 1.31\ rad \end{cases} \tag{3.7}$$

was performed, and the results are presented in Figure 3.8.

This simulation of the open loop ramp controller suggests that the chosen set point does not only correspond to a fixed point of the step-to-step map, as intended, but also was at least locally stable. To further investigate the possible stability of this open loop controller around the set point, we added a severe perturbation after

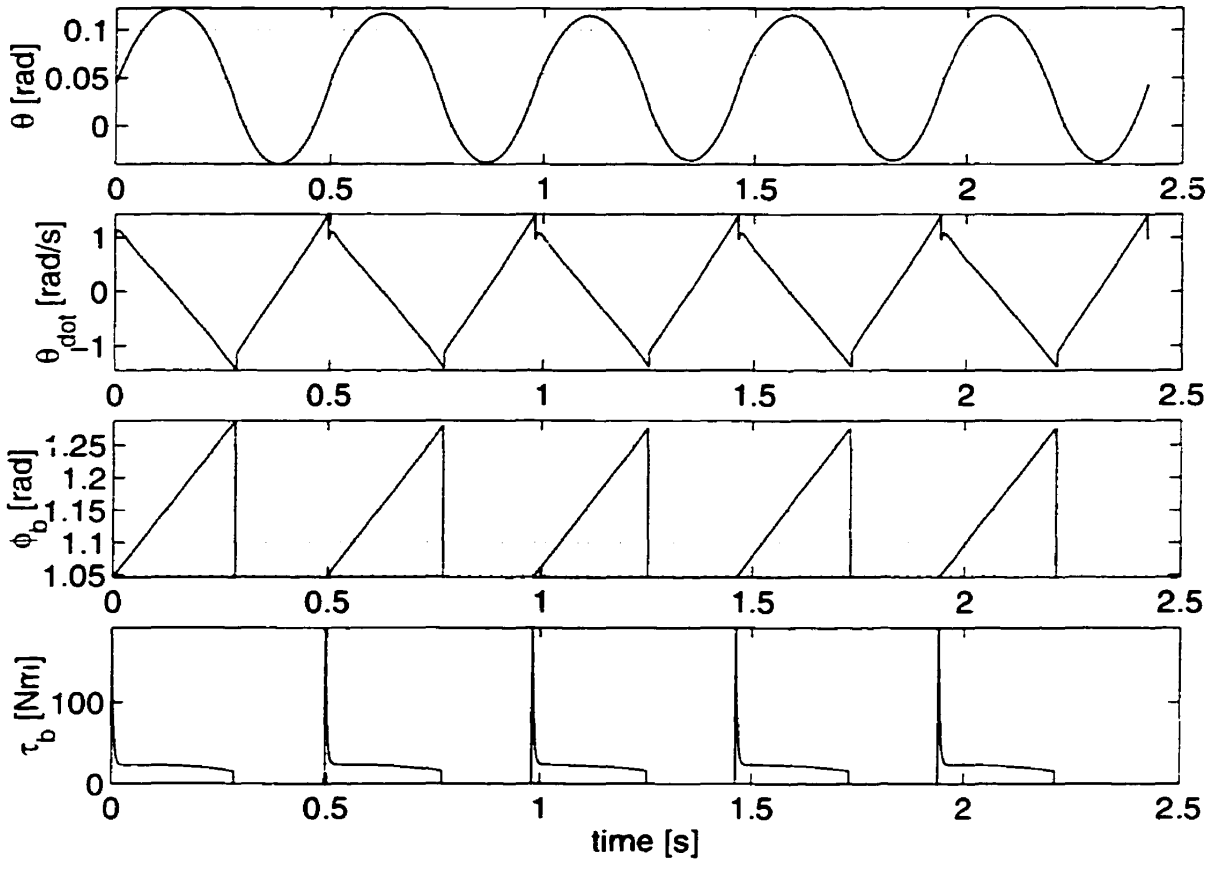


FIGURE 3.8. Stable motion produced by the open loop ramp controller

the first step, and, to our great surprise, the system converged rapidly back to the desired set point, $\dot{\theta}^{B+} = 1\ rad/s$. The response (resulting after-impact $\dot{\theta}^{B+}$) of the system to this disturbance is shown in Figure 3.9.

For a more complete insight into the range of initial body angular velocities which will converge to the desired set point (the domain of attraction of the controller), we plot the numerical evaluation of the step-to-step return map for the open loop ramp controller in Figure 3.10. This plot confirms the unusual and exciting fact that the open loop controller has a domain of attraction which is global for all practical purposes, from almost zero initial body angular velocity, to a maximum body angular velocity of $\dot{\theta}^{B+} = 2.3\ rad/s$, above which the robot would fall over backwards.

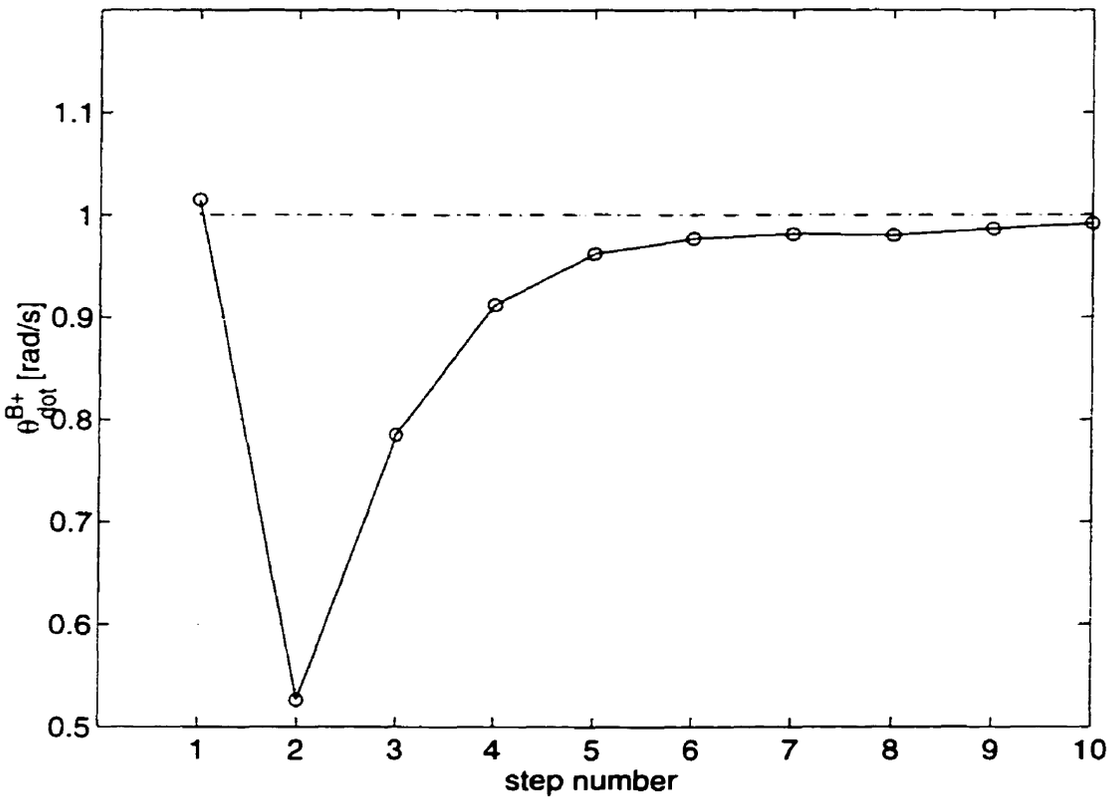


FIGURE 3.9. System response with open loop ramp controller after severe disturbance

As predicted by the return map (Figure 3.10), the open loop controller exhibits fast convergence to the fixed point, despite severe perturbations. In order to increase the convergence further, a feedback control will now be designed. There are several parameters that influence the behavior of the system:

- configuration when back leg impacts $(\phi_b^B, \phi_f^B)$,
- configuration when front leg impacts $(\phi_b^F, \phi_f^F)$,
- the constant angular velocity of the back hip $(\dot{\phi}_b)$ during back leg stance.

Given that the front leg remains fixed at all times $(\phi_f^F = \phi_f^B)$, and that the input angular velocity for the back hip will determine its final position $\phi_b^F$, there are three elements $(\phi_b^B,\ \phi_f^B,\ \dot{\phi}_b)$ that fully determine the resulting motion. At this time, we chose to maintain a fixed configuration at the back leg impact $(\phi_b^B,\ \phi_f^B)$, so that the only parameter that can still influence the behavior of the system is the back

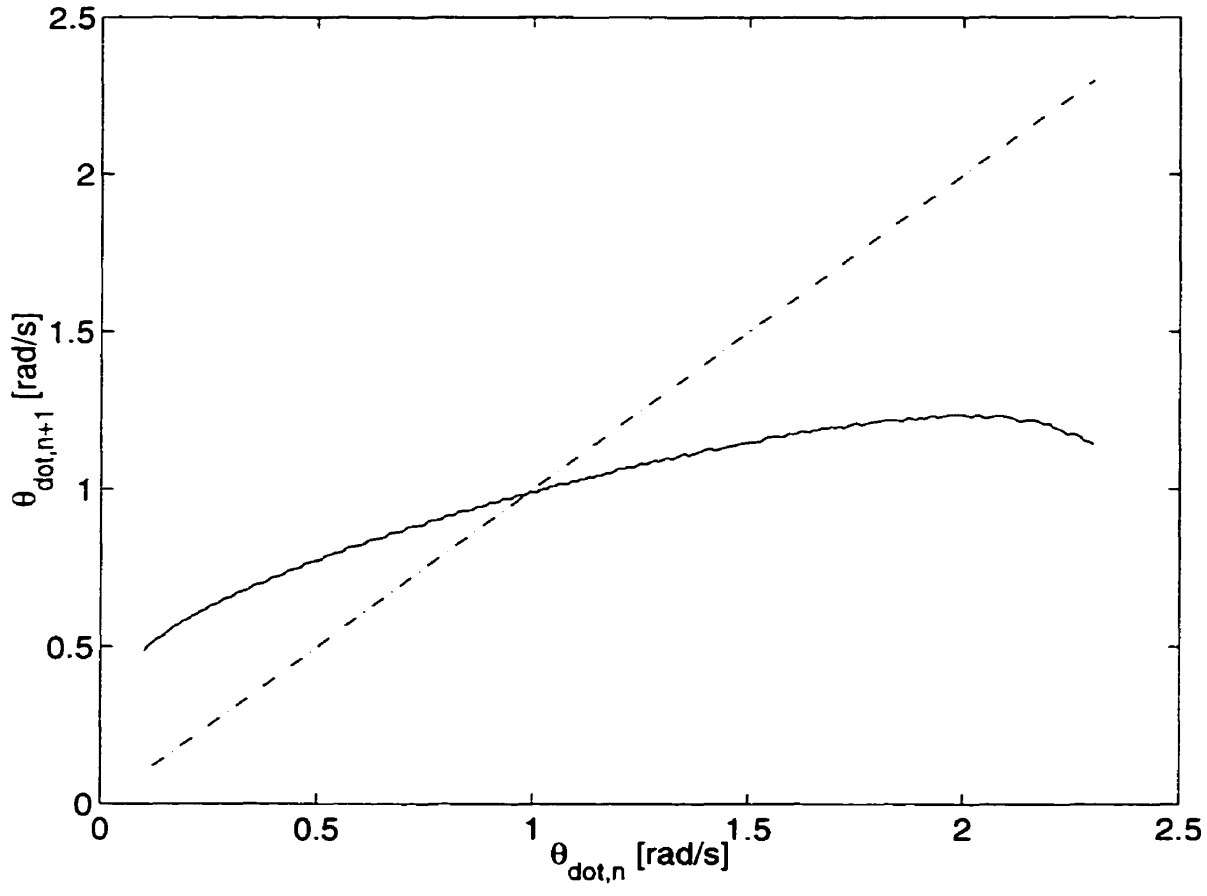


FIGURE 3.10. Numerical evaluation of the step-to-step return map for the open loop ramp controller

leg angular velocity. The feedback control will adjust the back leg angular velocity as a function of the initial body angular velocity $\dot{\theta}^{B+}$. For a range of after-impact body angular velocities $\dot{\theta}^{B+}$, and a range of back leg hip angular velocities $\dot{\phi}_b$, a look-up table has been generated. The input in this table is the actual (measured) $\dot{\theta}_n^{B+}$ and the output is the required $\dot{\phi}_b$ which, during the back leg support of the $(n+1)$ step, will result in the desired set point $\dot{\theta}_{n+1}^{B+} = 1 rad/s$. The look-up table has 180 entries (from $\dot{\theta}_n^{B+} = 0$ rad/s to $\dot{\theta}_n^{B+} = 1.79$ rad/s, in steps of 0.01 rad/s). For entries different from the tabulated values, a linear interpolation function is used to generate the outputs. This look-up table is used to simulate walking for several steps, with

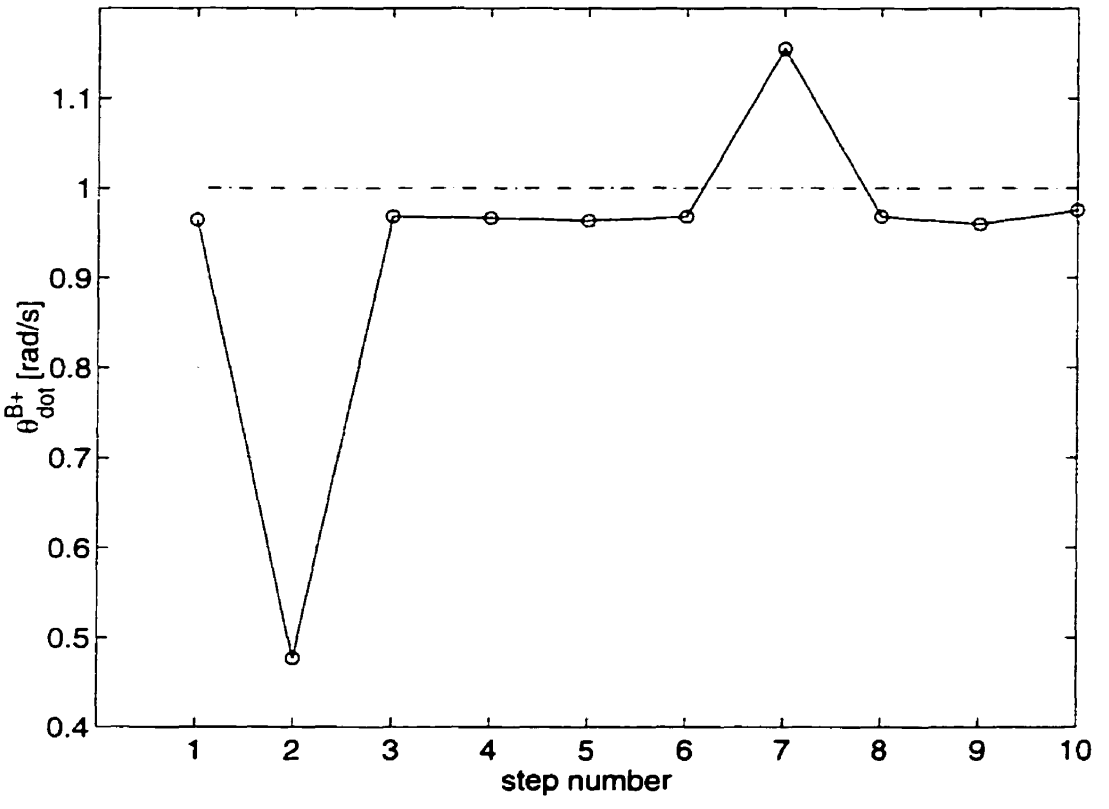


FIGURE 3.11. Closed loop motion shows one step recovery from disturbances

50% error in the $\dot{\theta}^{B+}$ (step 3) and 30% error for $\dot{\theta}^{F+}$ (step 7). As it can be seen in Figure 3.11 the recovery in both cases is accomplished in just one step.

Figure 3.12 shows that the feedback mechanism has an important effect on the stability. That is, the recovery from [-100% ; 80%] error between initial angular velocity of the body $\dot{\theta}^{B+}$ and the desired set point value is accomplished in just one step. This is indicated by the zero slope of the step-to-step return map in that range.

In Figure 3.8, the bottom graph shows the required back leg hip torque. These values will never be a realistic requirement when this controller is implemented on the experimental set-up. In order to perform simulations that reflect hardware limitations, we repeated the simulation shown in Figure 3.8 with the constraint $|\tau_b| \leq 40Nm$. The resulting stable behavior is presented in Figure 3.13, and it can be seen that, due to this torque limitation, there is a tracking error in $\phi_b$ (dashed line indicates the required trajectory and the solid line shows the actual value).

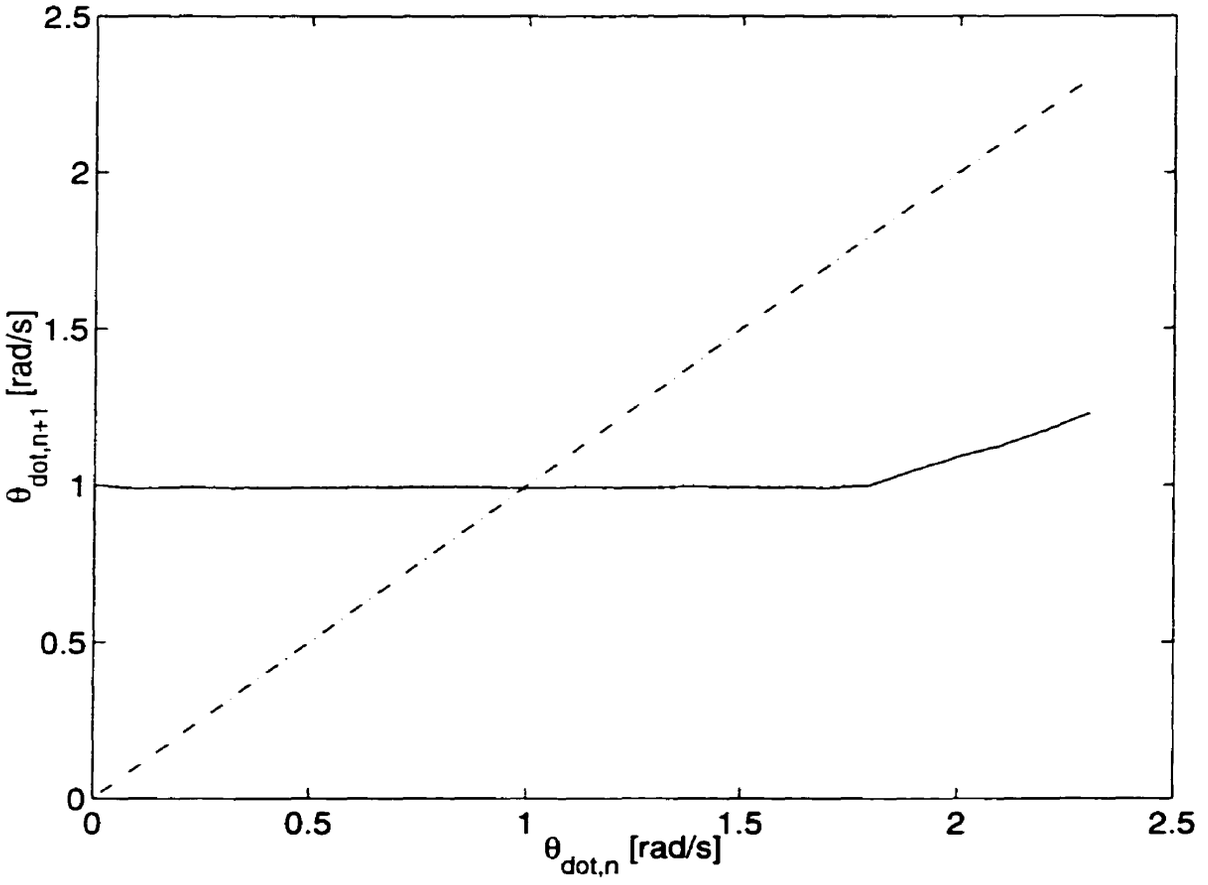


FIGURE 3.12. Step-to-step return map for closed loop (LUT) ramp controller

The analysis of the domain of attraction was necessary in order to investigate the stability of the system as a result of torque limitations. Figure 3.14 (solid line) shows that SCOUT, with no feedback information, and torque limitations, will be able to recover, in several steps, from a maximum error of 250% in the desired set point value. Figure 3.14 also includes (the dashed line) the domain of attraction presented in Figure 3.10. The comparison between the two curves indicates that hardware limitations imposed on the hip torques should not affect the system's stability.

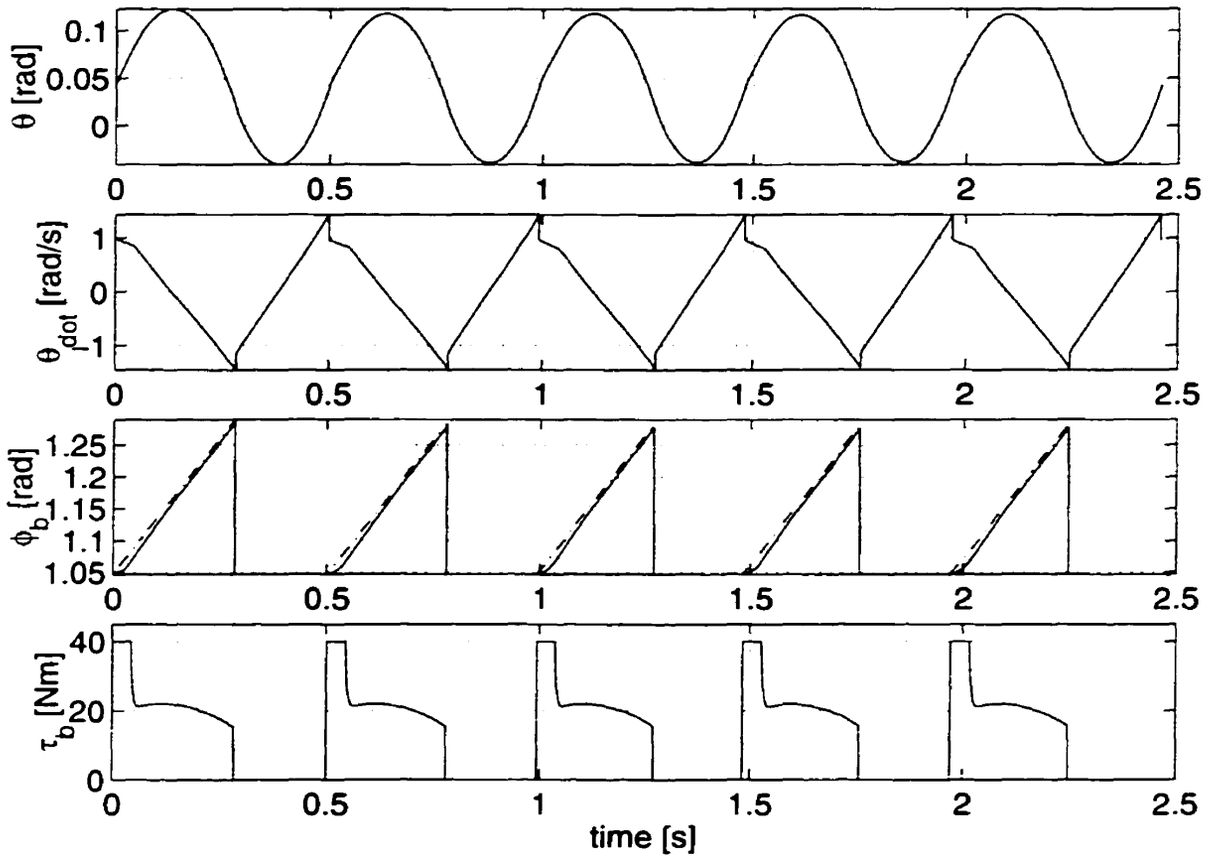


FIGURE 3.13. Stable motion produced by the open loop ramp controller, with added torque limitations

## 3.4. Saturated Ramp Controller

The results for the ramp controller presented in Section 3.3 show that the walking sequence will be characterized by small hip angle sweep, resulting in small steps (approx. 0.07 m). Furthermore, the required angular velocities for the back hip were almost five times lower than the limit imposed by the motors. In the ramp controller, the potential disturbances that occurred during the motion can be compensated by adjusting one parameter, $\dot{\phi}_b$. However, this can be a limiting factor for the feedback mechanism. Consequently, increasing the number of parameters that completely define the controlled input will result in potentially better performances of the feedback mechanism.

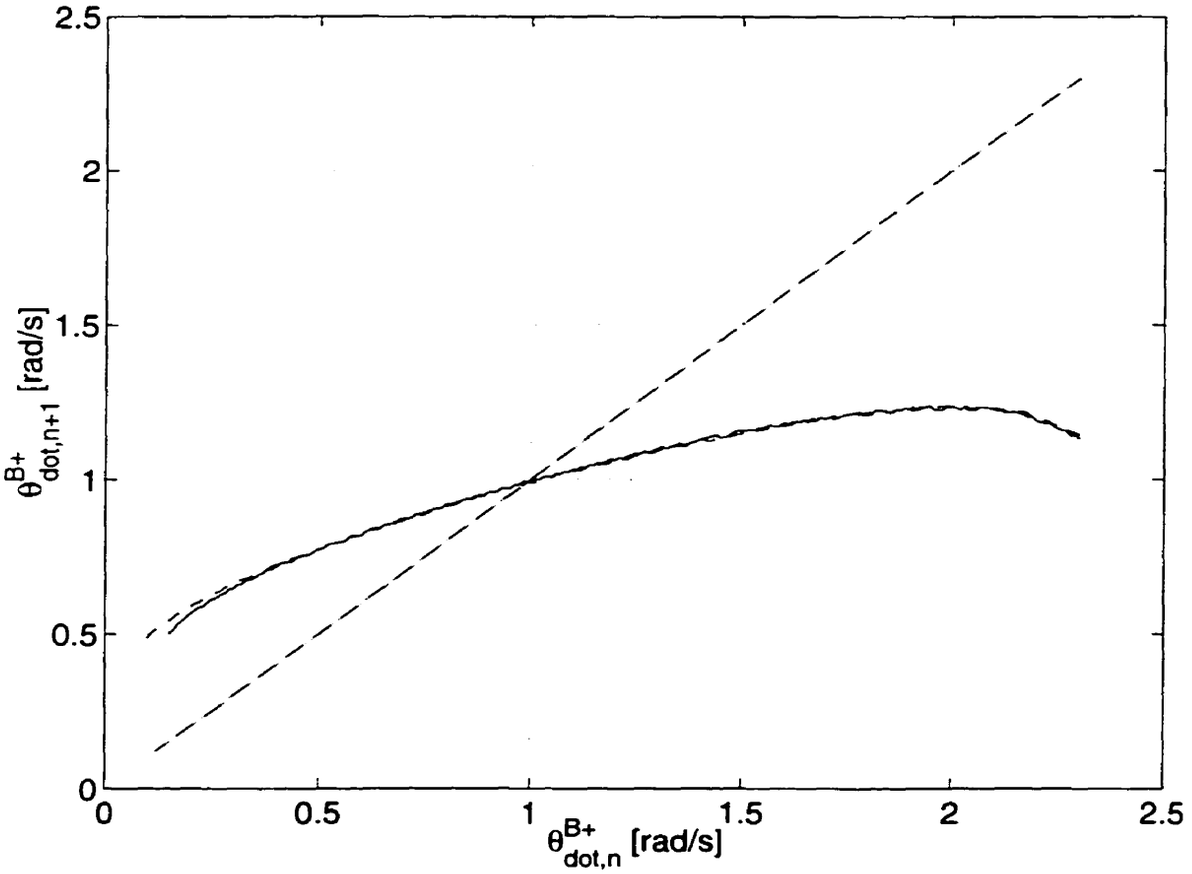


FIGURE 3.14. Step -to-step return map for open loop controller for the ramp controller with torque limitations (solid line) and without torque limitations (dashed line)

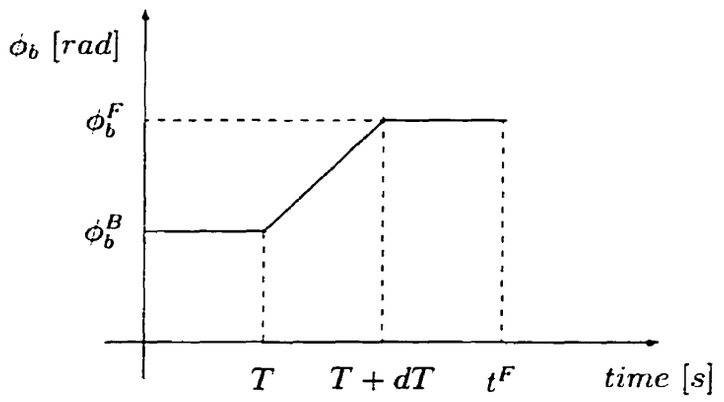


FIGURE 3.15. Saturated ramp input for the back hip angle

With these observations, we decided to try an approach in which the back leg had an imposed travel from $\phi_b^B$, $\phi_b^F$ (Figure 3.15). Using the considerations presented in Section 3.3, we decided to keep the front leg fixed throughout the motion (the actual value of this angle will be determined from simulations). In the back leg support phase, the back leg hip angle will be kept at a constant value for '$T$' seconds. In a given '$dT$' time the back leg hip angle will sweep between the desired limits $\phi_b^B$ and $\phi_b^F$, and remain at the final value for the rest of the back leg support. This controller is fully described by five parameters (as opposed to three in the ramp controller), namely,

- limits for the back leg sweep $(\phi_b^B, \phi_b^F)$
- front leg orientation $(\phi_f^F)$
- time at which the actuation on the back leg begins $(T)$
- $\dot{\phi}_b$ (or equivalently $dT$ shown in Figure 3.15).

In order to simplify the analysis we will keep a fixed configuration at the moments of support exchange, as we did in the ramp controller algorithm. That leaves us with two parameters that will fully determine the input, namely $[T, \dot{\phi}_b]$. We chose again $\phi_b^B = 1.05\ rad, \phi_f = 1.31\ rad$, and, to avoid slipping during the experiments, $\phi_b^F = 1.83\ rad$.

With the input defined by two parameters ($[T, \dot{\phi}_b]$), a simulation was used in determining the combination of the two parameters that will yield a periodic motion ($\dot{\theta}_{n+1}^{B+} = \dot{\theta}_n^{B+}$). The simulation involved a numerical search in a two dimensional space. The range for the first search direction, $T$, was set to [0;0.1s], and, for the second search direction, $\dot{\phi}_b$, [2 rad/s; 8 rad/s] (the upper limit for the $\dot{\phi}_b$ range is dictated by the hardware limitations). For each point in the search space, the mathematical model was integrated, and the results are shown in Figure 3.16. The data points (denoted by 'o') on each curve are obtained for different back hip angular velocities $\dot{\phi}_b$; moreover, each curve corresponds to a certain value of $T$ (see Figure 3.15). Apparently, the effect of the $T$ and $\dot{\phi}_b$ parameters on $\dot{\theta}_{n+1}^{B+}$ is minimal. Also, with the current settings, according to Figure 3.16, starting with $\dot{\theta}^{B+} = 1\ rad/s$, the next step

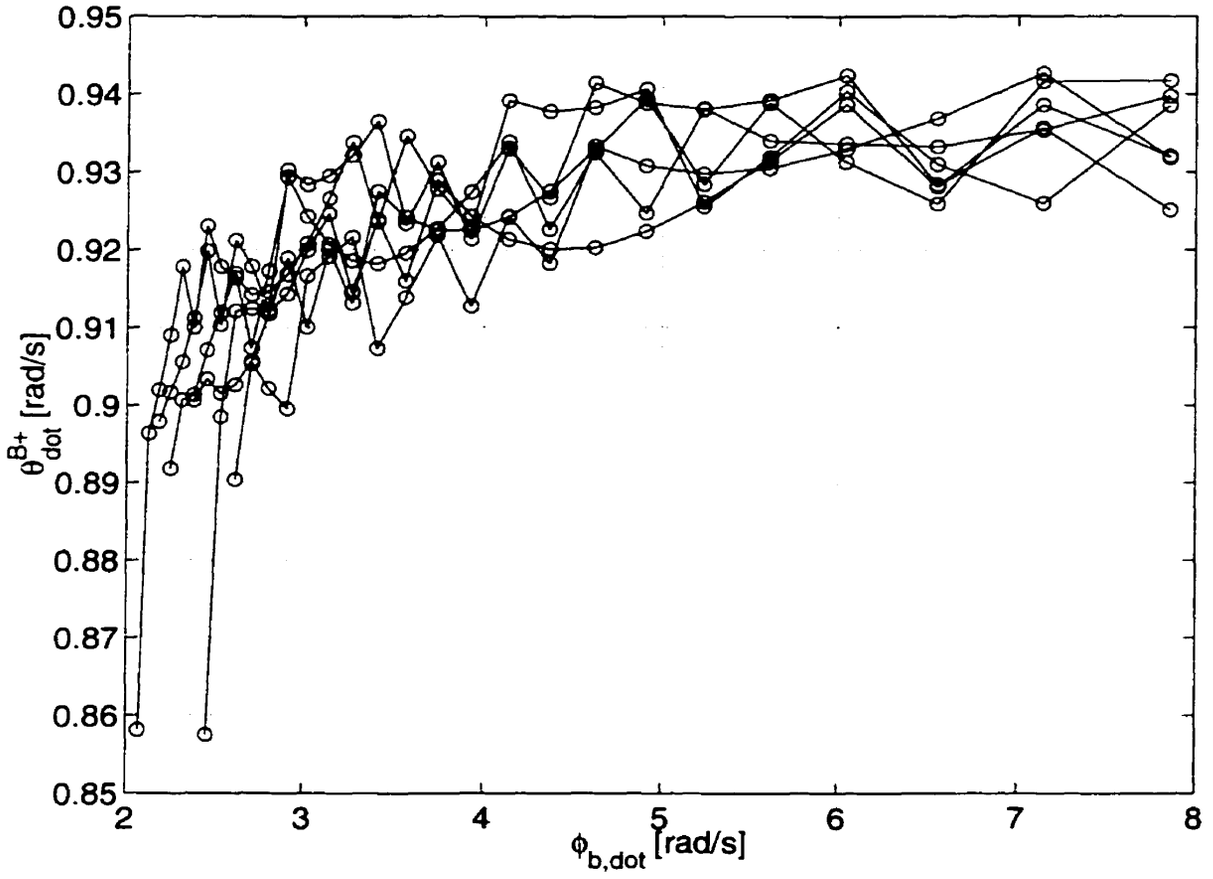


FIGURE 3.16. Range of possible $\dot{\theta}^{B+}_{n+1}$ for $\dot{\theta}^{B+}_{n} = 1.0\ rad/s$

will be characterized by $\dot{\theta}^{B+} \approx 0.93\ rad/s$ for a large range of $\dot{\phi}_b$. This violates the periodic motion condition ($\dot{\theta}^{B+}_{n} = \dot{\theta}^{B+}_{n+1}$). However we simulated the motion of our system having the desired set points,

$$\begin{cases} \phi^B_b &= 1.05 \quad rad \\ \phi^F_b &= 1.83 \quad rad \\ \dot{\phi}_b &= 3.30 \quad rad/s \\ T &= 0.00 \quad s \\ \phi_f &= 1.31 \quad rad. \end{cases} \tag{3.8}$$

As depicted in Figure 3.17, the open loop motion is stable around a set-point $\dot{\theta}^{B+}_{n} = 0.93\ rad/s$. The step to step return map, presented in Figure 3.18, confirms

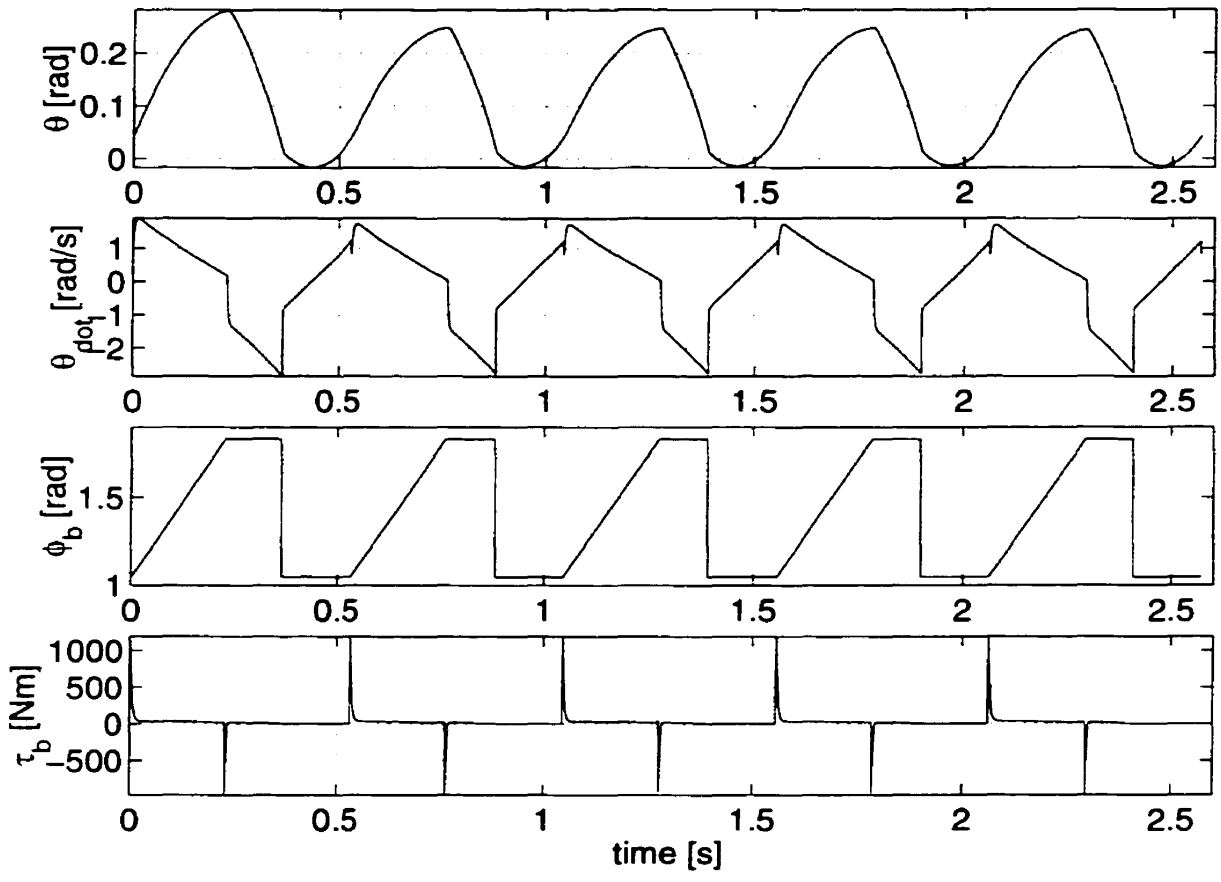


FIGURE 3.17. Periodic motion resulted from the open loop saturated ramp controller

that the convergence set-point is at the mentioned value. The domain obtained for this type of controller is different from the one presented in Figure 3.10, and suggests that, even with an open loop control algorithm, any disturbance (unless it causes turn over) in $\dot{\theta}^{B+}$ is compensated in one step.

To illustrate this, we simulated the walking for ten steps, and added a 50% error in $\dot{\theta}^{F+}$ (step 3) and in $\dot{\theta}^{B+}$ (step 7). As expected, the recovery was complete in just one step. As a conclusion, even if our control algorithm does not use any feedback information, we demonstrated that the recovery from disturbances can be done in just one step. Therefore, the design of a closed loop control algorithm based on a saturated ramp function for $\phi_b$ it is not necessary.

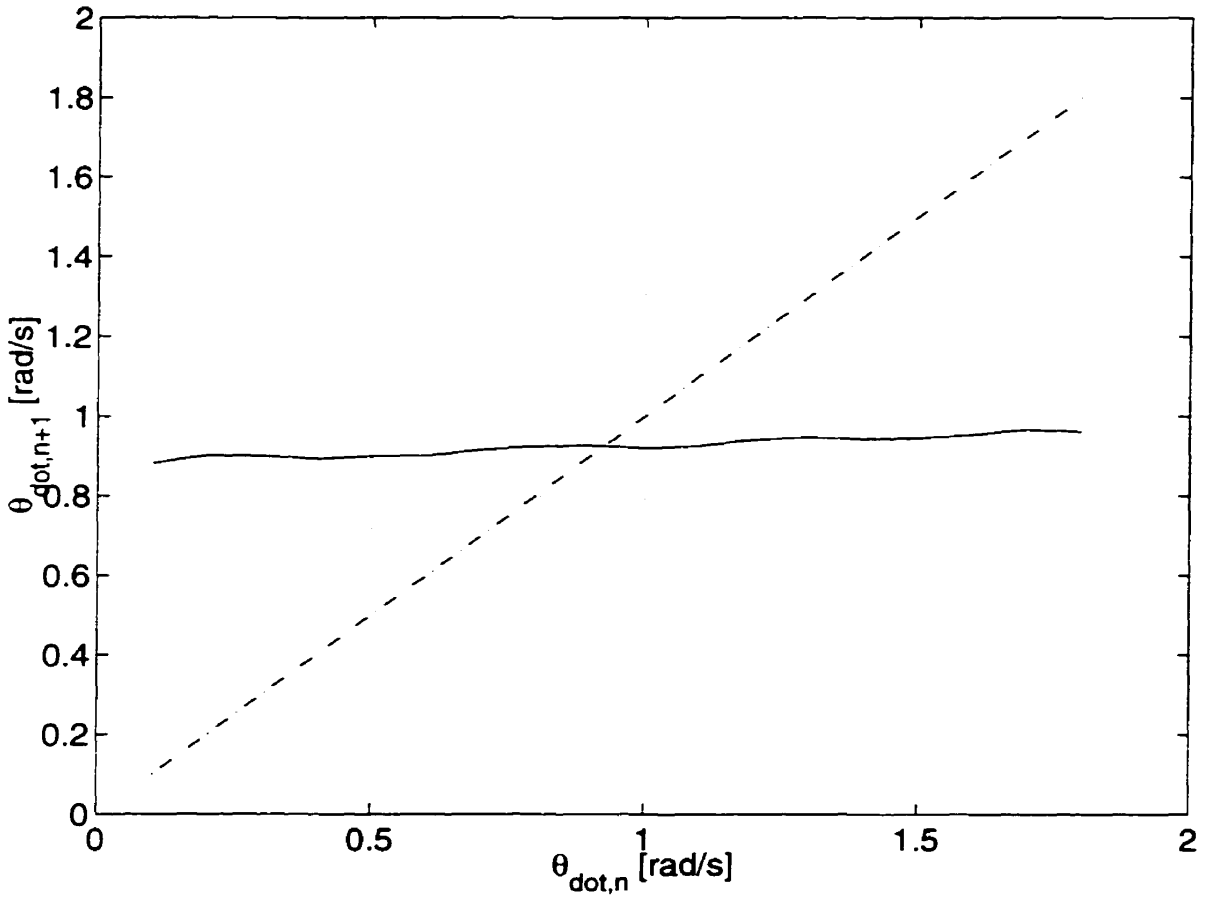


FIGURE 3.18. Step-to-step return map

In Figure 3.17 is shown the back hip actuator torque requirements. Limiting this torque at $|\tau_b| \leq 40Nm$ will result in tracking errors for $\phi_b$ leading to a premature front leg impact (back leg did not complete its sweep). As a consequence, a fixed point of the step to step return map was not found. This suggested to us that the implementation of this controller will not be successful.

## 3.5. Summary and Conclusions

Three different control algorithms have been proposed. The polynomial controller is a scheme in which the length of the supporting virtual leg is controlled via a third order polynomial in body angle. The polynomial coefficients are determined from the initial and final conditions. The final linear velocity for the virtual leg is

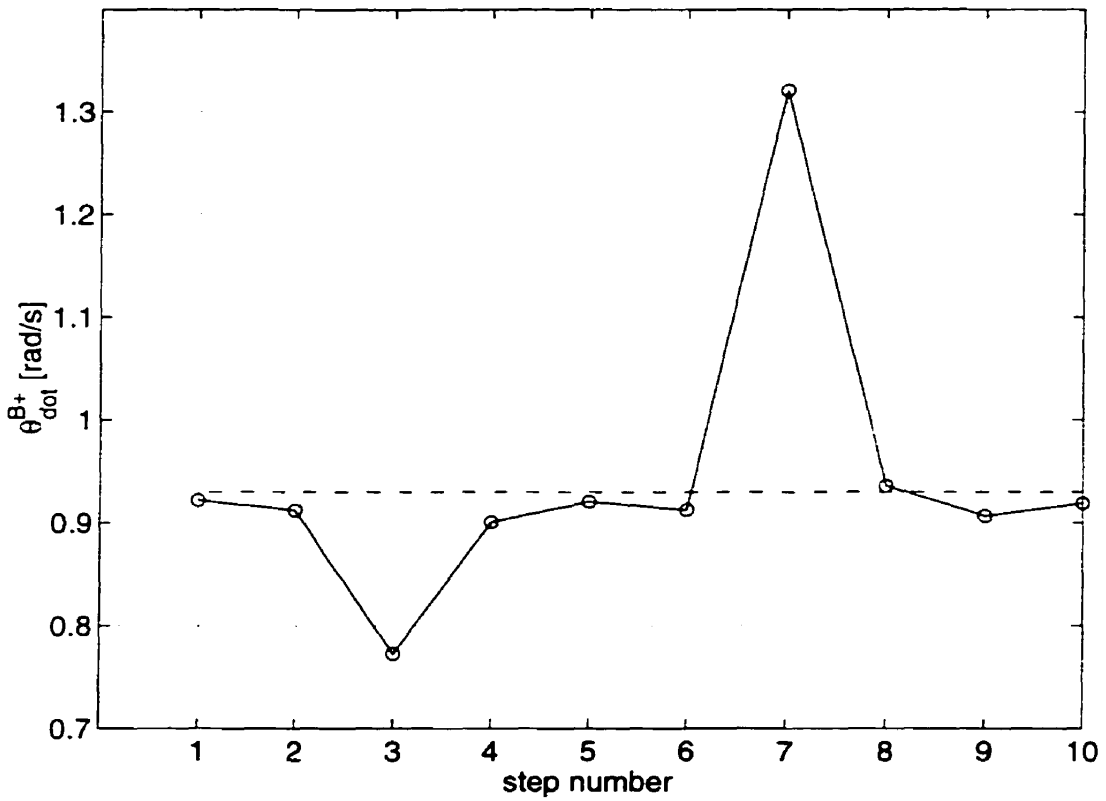


FIGURE 3.19. Open loop motion shows one step recovery from disturbances in $\dot{\theta}^{B+}$

imposed so that a certain value for the after-impact angular velocity is obtained. The polynomial coefficient calculations also involved the value of the body angular velocity at touch down time. Given that this value is influenced by the applied controller, assumptions had to be considered in determining this touch down body angular velocity. If accurate predictions were considered for $\dot{\theta}^{F-}$, $\dot{\theta}^{B-}$, the resulting after-impact body angular velocity had exactly the desired set point value; if coarser predictions about $\dot{\theta}^{F-}$, $\dot{\theta}^{B-}$ were made, a constant error between the desired set point and obtained value was observed. However, in both cases (accurate or coarser $\dot{\theta}^{F-}$, $\dot{\theta}^{B-}$ prediction), numerical simulations indicated that both stable and periodical walking will be obtained.

During experimental implementation of the polynomial controller on SCOUT I hardware limitations (available torque and speed) indicated the need for simpler

control schemes. Moreover, the actuation should be distributed during the stance phase. A very simple control algorithm was used in the ramp controller. We proposed a ramp input for the supporting hip angle. Simulation results indicated that only the sweep at a constant angular velocity of the back leg had a positive effect on both forward displacement and transfer of momentum. Therefore, in this control scheme the front legs are fixed all the times. The parameters (identified as the *walking parameters*) that need to be specified for the ramp controller are the hip angles at back leg and front leg impact moments and the back leg constant angular velocity while on back leg support. The walking parameters have been determined through a series of simulations using the desired set point ($\dot{\theta}^{B+} = 1\ rad/s$) and the periodic motion condition ($\dot{\theta}^{B+}_{n+1} = \dot{\theta}^{B+}_{n}$). It has been shown that, even with the determined walking parameters an open loop motion is stable and converges towards the desired set point. Next, a look up table was used as a feedback mechanism, to determine the appropriate back leg angular velocity ($\dot{\phi}_B$) as a function of the measured after-impact body angular velocity ($\dot{\theta}^{B+}$). The feedback is introduced with the purpose of reducing the number of steps required to recover from possible disturbances and increasing the range of disturbances from which the system can recover in one or several steps. The entry in this look up table is $\dot{\theta}^{B+}_{n}$ and the output is the necessary back leg hip angular velocity that will yield $\dot{\theta}^{B+}_{n+1}$ at the set point value, or very close to it. In order to make our simulations more realistic, torque limitations have been introduced in the mathematical model. However, these limitations did not influence either the performance of the system or its stability noticeably.

The performance given by the ramp controller indicated that SCOUT will take short steps. That is why we changed the controlled input to a modified saturated ramp function. Using this control scheme, one will have control over the step size through the limits defining the saturated ramp. In this new control scheme, the back leg will end its sweep motion before the front leg impact occurs. Hence, the after-impact angular velocity $\dot{\theta}^{B+}$ will be a result of only the before-impact angular velocity $\dot{\theta}^{B-}$. As in the ramp controller, simulations showed that the contribution of

the front leg to the overall motion is most effective if it is kept at a fixed position. The same set point ($\dot{\theta}^{B+} = 1\ rad/s$) was considered and walking parameters have been determined via numerical simulations. The stability analysis indicated that this type of control algorithm has a fast convergence (one step) towards the desired set point, even when an open loop control algorithm is used. However, the required torques attain much larger peak values than those observed in the ramp controller simulations. This indicated potential problems in implementing this type of controller on the experimental set-up.

# CHAPTER 4

# EXPERIMENTAL RESULTS

## 4.1. Experimental Set-up

SCOUT II is a quadruped robot with a mass of 27 kg and measures 0.275 m in height, 0.552 m in length and 0.48 m in width. The legs are basically rigid sticks and connect to the body through rotational joints. Each joint is driven independently by the combination of DC motors, reduction gear set and timing belt. Given that during walking important impacts will occur, each leg's toe is protected by a rubber ball.

Two laser sensors are added at the front and back of body for body angle measurements. On each motor shaft optical encoders are mounted and are used to measure the hip angles. Furthermore, current measurements from each motor amplifier indicate the actual applied torques. Inside the legs, linear potentiometers are mounted, and used in detecting the contact with the ground. Hall effect sensors are used to calibrate the offsets for the incremental hip angle sensors.

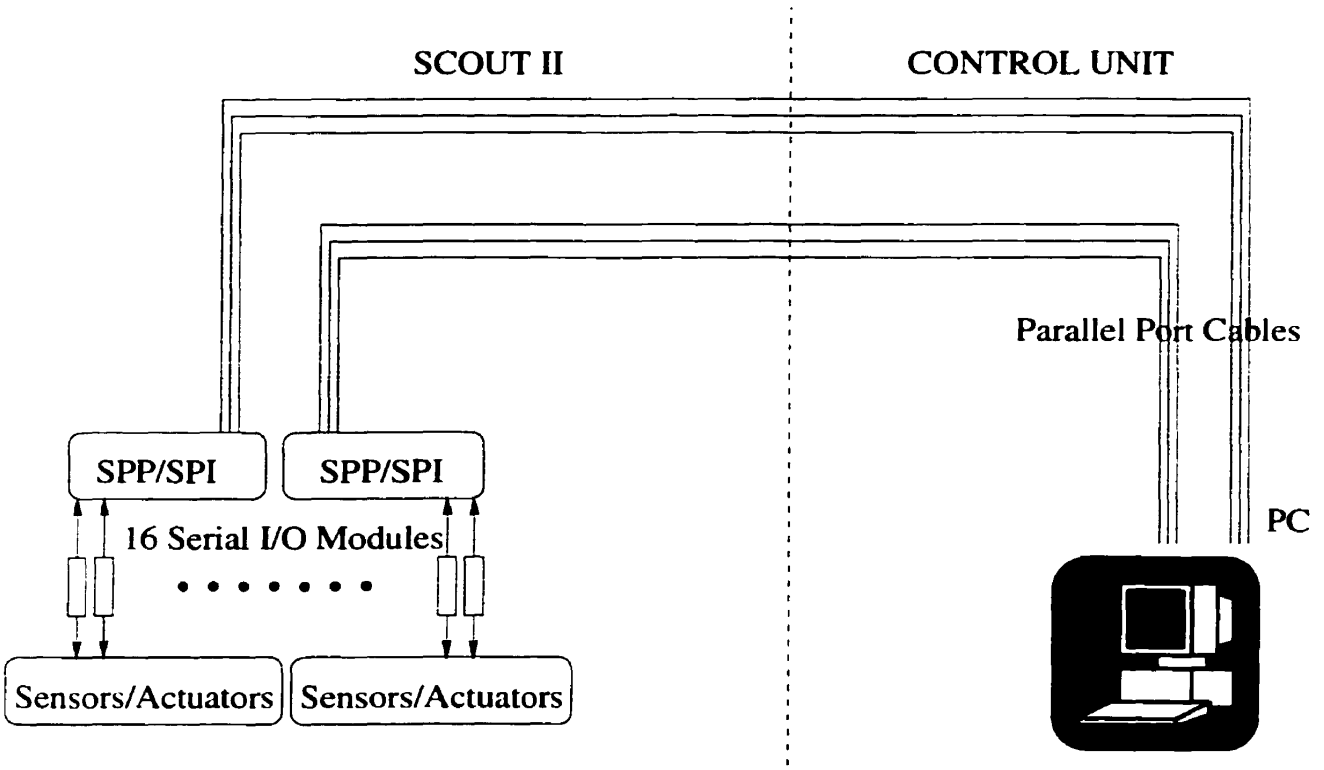


FIGURE 4.1. Schematics of experimental set-up

SCOUT II is controlled by a PC, running under the QNX environment [**9**]. The control algorithms are implemented in the experimental code, where a PD controller, with optional feedforward terms, will track the desired reference trajectory for the hip angles. The interconnection between the control unit (PC) and SCOUT II is sketched in Figure 4.1. The Standard Parallel Port / Serial Peripheral Interface (SPP/SPI) is the interface between the PC and peripheral serial I/O modules.

## 4.2. Ramp Controller

The ramp controller described in Section 3.3 has been implemented on SCOUT II. The configuration at the moments of exchange of support and required back actuator angular velocity were set according to eq. (3.7).

In performing the simulations, the mathematical model developed in Chapter 2 was used (see Figure 3.1). It was mentioned in the previous chapters that a dynamic walking sequence would be designed and implemented, hence SCOUT would be either on its back or front leg. However, during the experimental work, it was clear that there existed a non-negligible double stance phase. No control algorithm has been developed for the double stance, so two alternatives were available,

- after back leg impact, even if SCOUT is still in double stance, start the designed control algorithm (a ramp or a saturated ramp); or,
- keep the hip angles at their prescribed position ($[\phi_b^B; \phi_f^B]$ or $[\phi_b^F; \phi_f^F]$) until the single support phase is detected.

In implementing the ramp controller, we used the first alternative, which led to stable walking, as presented in Figure 4.2. In the top two graphs, different symbols were used to delimit the beginning of different states: 'o' start of back leg support, '*' of double stance phase and '+' for front leg support. These delimiters show that during the experiments the double stance accounts for approx. 20% of the step time. The effect of this double stance is one of the factors that can explain the differences between the simulations (Figure 3.13) and the experimental results (Figure 4.2).

In designing a control algorithm the controlled momentum transfer idea was considered with the goal of obtaining a periodic motion. From the experiments it has been observed that the periodic motion condition has been satisfied. Hence, it is still needed to validate the mathematical model derived for the impact of either back or front leg.

We performed two different sets of experiments. In one of them SCOUT II walked on our linoleum tile covered laboratory floor, and in the other one on carpet. The purpose of these two experiments was to analyze the effect of toe slipping on the ground on the momentum transfer, given that the mathematical model considers the toe to be pin connected to the ground after the impact. For these two different

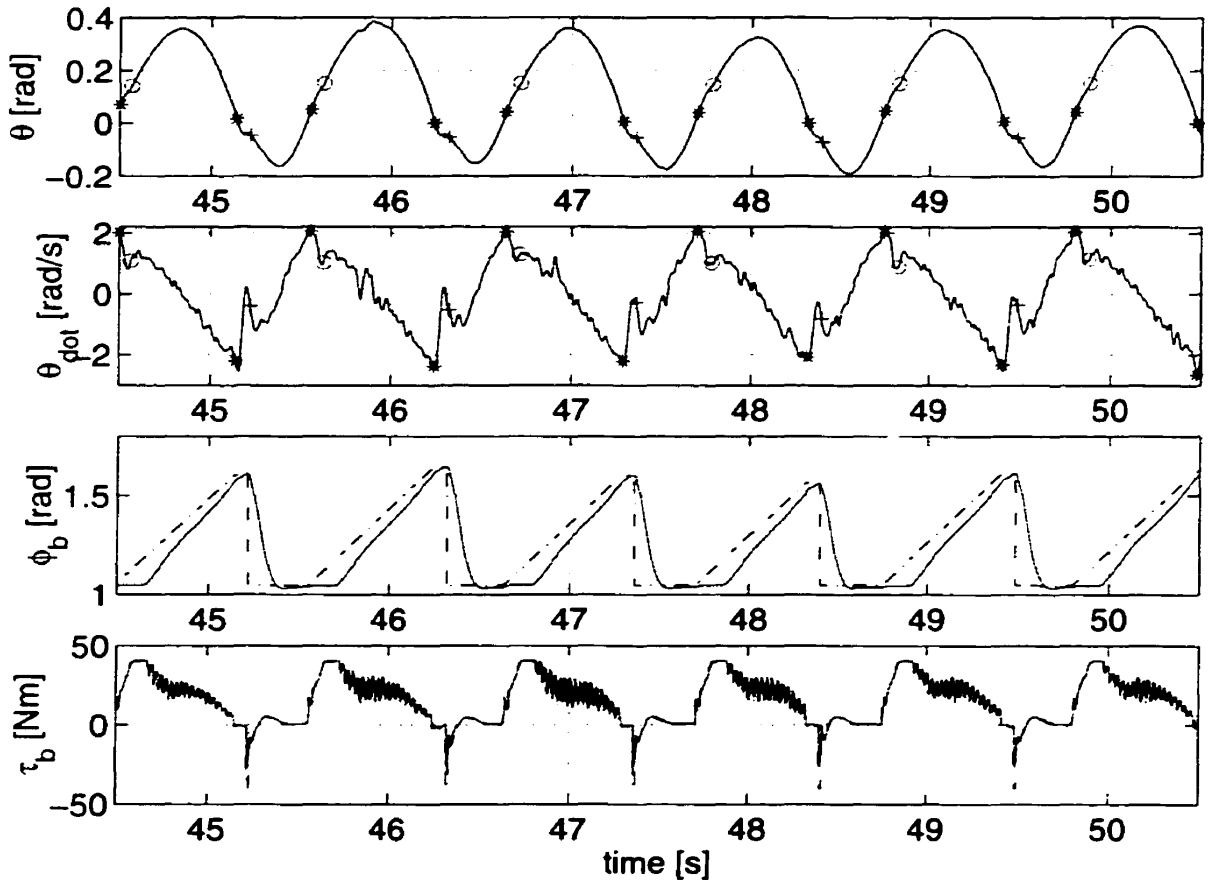


FIGURE 4.2. Experimental results for ramp controller ; '*' indicates the beginning of the double stance phase; 'o' indicates the beginning of the back leg support and '+' the beginning of the front leg support; the dashed line indicates the desired value and the solid line the actual value

experiments, the states at the end of the single stance and beginning of the next single stance were recorded. Using these states the theoretical value for the angular velocity $\dot{\theta}^{F+}$ ($\dot{\theta}^{B+}$) was compared to the experimental value.

Figure 4.3 shows the predicted (represented by a 'o') and experimentally obtained ('*') value for $\dot{\theta}^{B+}$. The left graphs (a) correspond to the experiments on the linoleum floor, and the right graphs (b) are obtained from the experiments done on the carpet. As it can be observed, the effect of increased friction between the toe and the ground decreased the error between the theoretically predicted value and the actual value. Furthermore, the $\dot{\theta}^{B+}$ values obtained from the experiments on the carpet, were closer

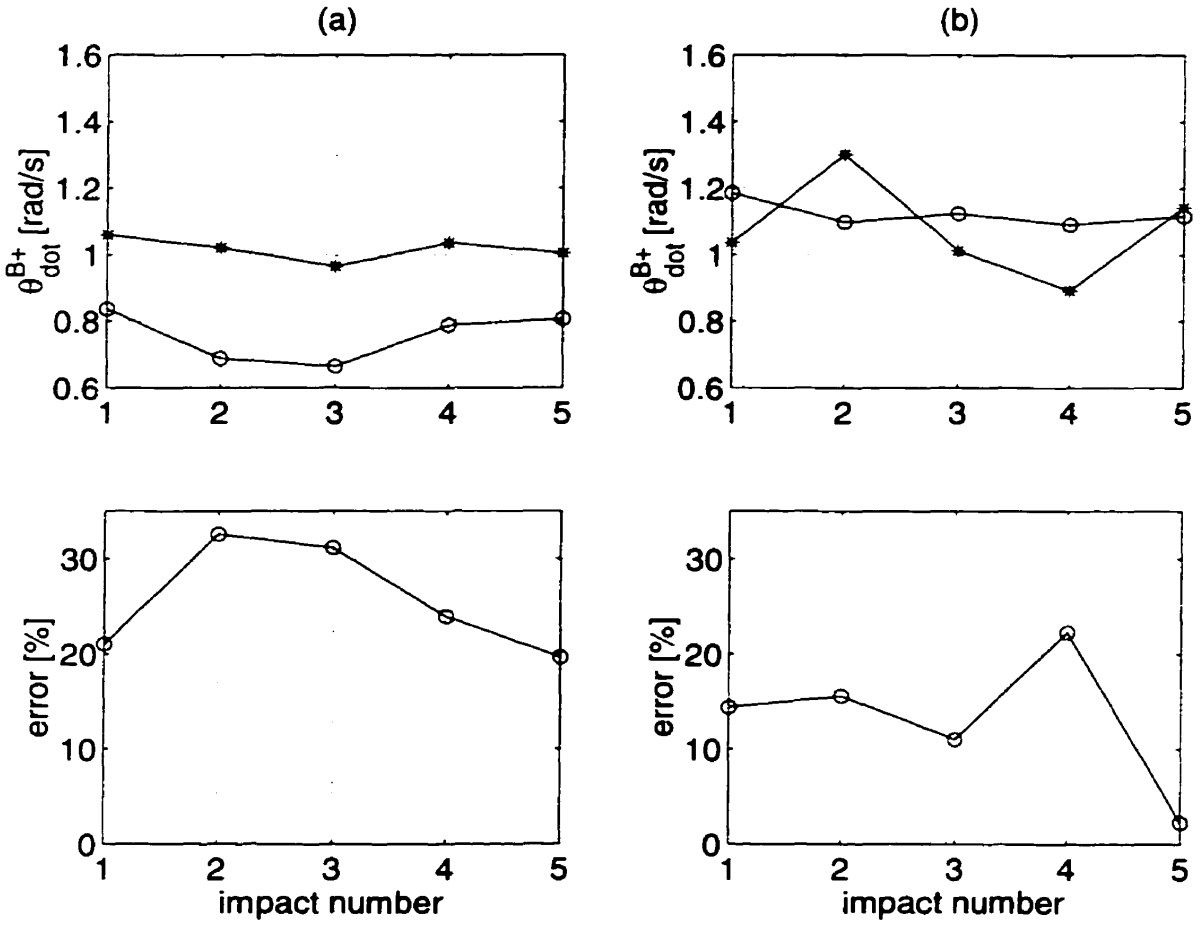


FIGURE 4.3. Back leg impact momentum transfer (a) on linoleum tiles and (b) on carpet ['o' theoretical value; '*' experimental value]

to the desired set point value $\dot{\theta}^{B+} = 1\ rad/s$. In this control algorithm, the back leg is still sweeping when the front leg impact occurs. Hence, at front leg impact, the effect of toe slipping on the ground is more evident due to the large forward body linear velocity. In the experiments conducted on linoleum floor the resulting $\dot{\theta}^{B+}$ is larger than its theoretically predicted value. This indicates that the dynamics of the double stance and the actuation strategy during the double stance have an important effect on the momentum transfer, an effect which our mathematical model did not take into account.

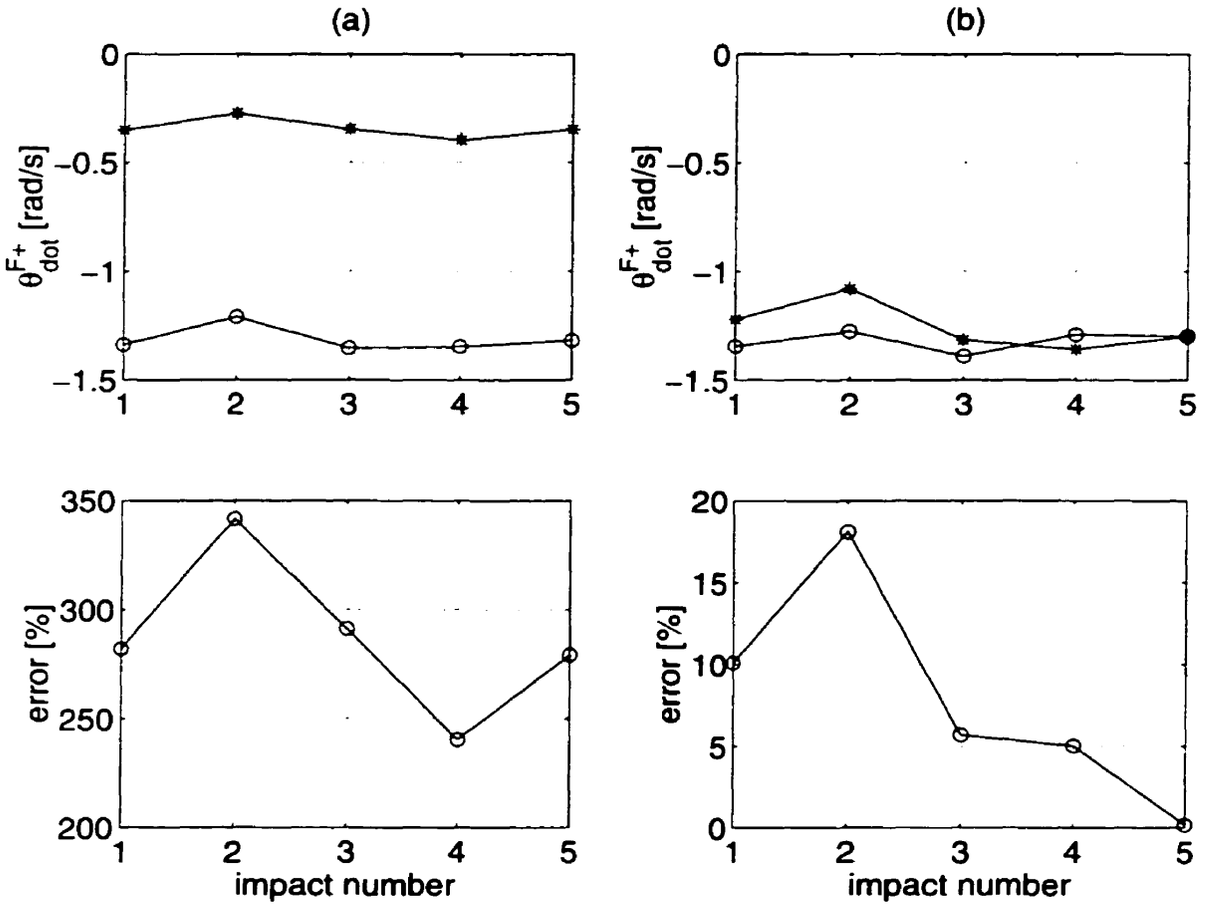


FIGURE 4.4. Front leg impact momentum transfer equation (a) on linoleum tiles and (b) on carpet ['o' theoretical value; '*' experimental value]

The same experiment revealed even more drastic differences for the front leg impact. The left graphs (a) presented in Figure 4.4 (corresponding to the experiments performed on the linoleum tile floor) show the important difference between the theoretical predicted value (denoted by 'o') and the experimental one ('*'). The right graphs (b) (obtained from the experiments performed on the carpet) emphasise the importance of preventing toe slippage, where we get fairly good correspondence between the experimental and theoretical values. On linoleum tiles (Figure 4.4(a)), toe slippage occurs and causes the loss of most of the body angular momentum. Figures 4.3 and 4.4 show that the impact of the front legs is more sensitive to the slippage

effect. During the motion, only in the back leg support phase there is an actual forward displacement of the body. This forward motion increases the slippage effect at the impact of the front legs.

## 4.3. Saturated Ramp Controller

Another set of experiments have been dedicated to the implementation of the saturated ramp controller described in Section 3.4. With the parameters set according to eq. (3.8) and no actuation during double stance, the resulting stable motion is shown in Figure 4.5.

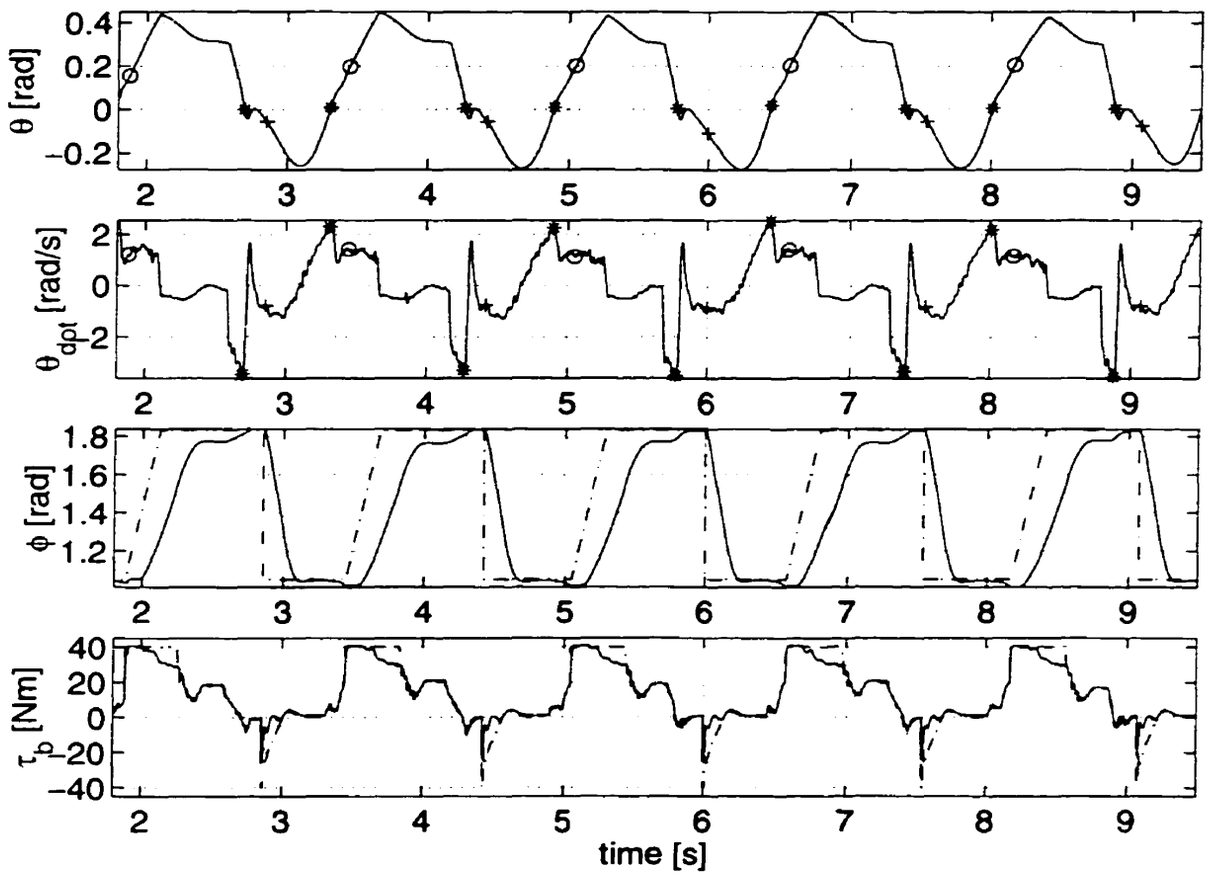


FIGURE 4.5. Experimental results for ramp controller ; '*' indicates the beginning of the double stance phase; 'o' indicates the beginning of the back leg support and '+' the beginning of the front leg support; the dashed line indicates the desired value and the solid line the actual value

As predicted from the numerical simulations, tracking problems have an important effect on the experimental implementation. The third graph presented in Figure 4.5 shows the difference between the required back leg hip angle (dashed line) and the actual one (solid line). Again we have delimited different stages ('o' beginning of back leg support, '*' beginning of double stance, '+' beginning of front leg support) to emphasise the importance of the double stance time. Furthermore, in the third graph one can observe that the back leg is still in motion when front leg impact occurs. This poor tracking is a direct result of the hardware limitations on the maximum torque that can be delivered by the hip motors. Furthermore, the bottom graph presented in Figure 4.5 shows that even when a peak torque is required (dashed line) the delivered value (solid line) is not always the required value (again due to hardware limitations). This experiment showed that, despite the poor tracking, a periodical motion has been obtained.

In Figure 4.6 we analyse the momentum transfer for front leg impact (a) and back leg impact (b). As mentioned before, the back leg is still moving when front leg impact occurs; hence the front toe slippage is increased by the body forward velocity (this experiment has been conducted on the linoleum floor). The slippage combined with the effect of the double stance are the major elements that can explain the large differences between the theoretically predicted $\dot{\theta}^{F+}$ (represented by 'o' in Figure 4.6(a)) and the experimentally obtained value ('*' in the same figure). When back leg impact occurs, the slippage of the back toe is less significant; hence, lower errors between theoretical and experimental values for $\dot{\theta}^{B+}$ (Figure 4.6(b)). However, the resulting $\dot{\theta}^{B+}$, in the range of [1.1; 1.4] rad/s, is away from the desired set point value $\dot{\theta}^{B+} = 1\ rad/s$.

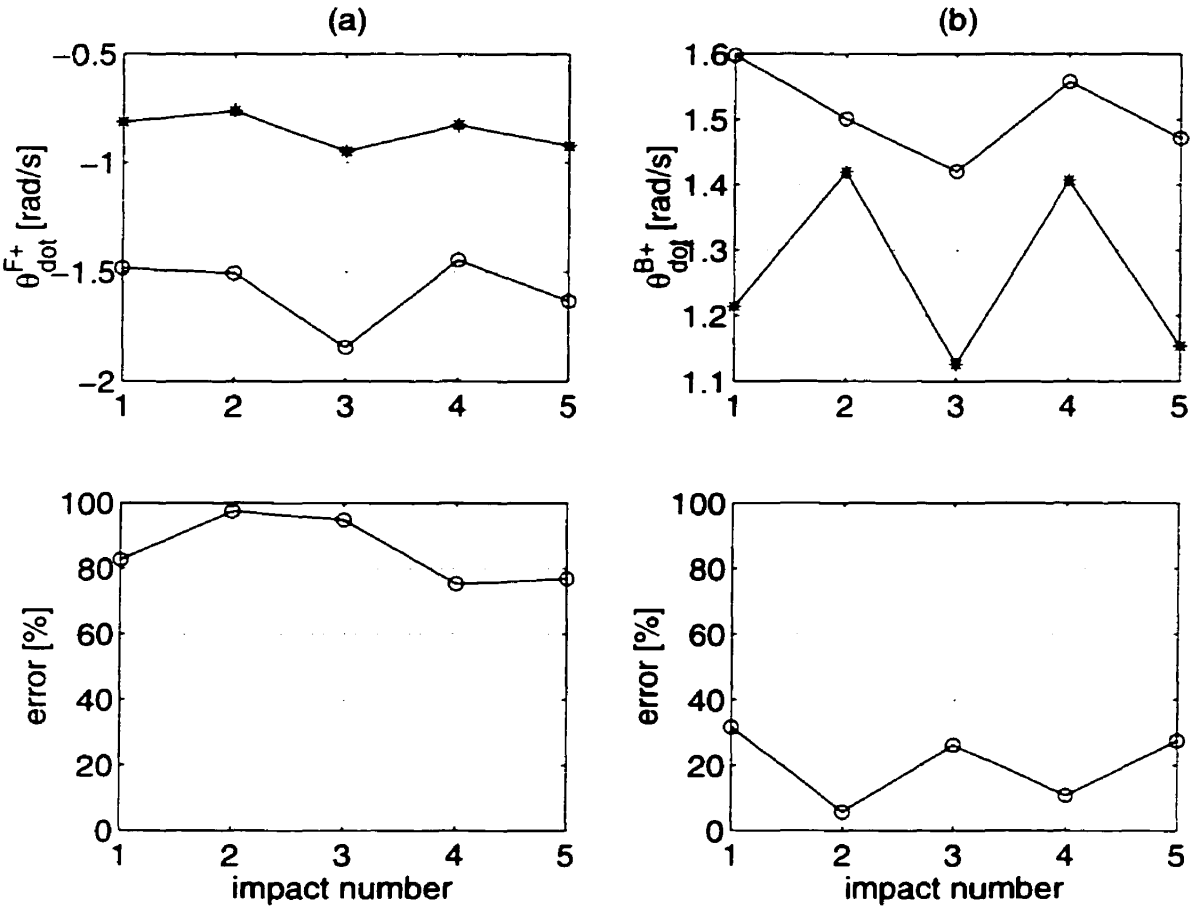


FIGURE 4.6. Momentum transfer at (a) back leg impact and (b) front leg impact['o' theoretical value; '*' experimental value]

## 4.4. Summary and Conclusions

This section presented the experimental results obtained from the implementation of the ramp controller and saturated ramp controller. Both experiments resulted in periodic motion.

When implementing the ramp controller, two different sets of experiments have been conducted; one on standard laboratory linoleum tiles, one on carpet. These experiments showed the disastrous effect of toe slippage on the momentum transfer when walking on linoleum tiles. Carpet floor reduced toe slipping without completely eliminating it. The experiments used to validate the saturated ramp controller were

conducted only on linoleum floor. These experiments were clearly influenced by poor tracking in the desired input trajectory and important toe slipping.

Tracking problems and significant double stance time were present in both controller implementations; however, in the ramp controller the tracking error resulted in an error only in the final value for the hip angle, not its angular velocity. That is why the set point $\dot{\theta}^{B+} = 1\ rad/s$ used in developing the theoretical simulations was observed, within an acceptable range, in the experiments as well (see Figure 4.3(b)). The same set point $\dot{\theta}^{B+} = 1\ rad/s$ was used in designing the saturated ramp controller, and Figure 4.6 shows its experimentally obtained value. Still, this experimental value is the result of the combined effect of an error in the final hip angle and the presence of the hip angular velocity.

As a conclusion, it has been observed that implementing a very simple control algorithm, the ramp or saturated ramp controller, one can obtain a periodic motion. Experimental results showed that the ramp controller is easier to implement, because it requires less actuator torque.

# CHAPTER 5

# CONCLUSIONS

## 5.1. Summary

This thesis presented walking control algorithms for a new class of dynamically stable legged robots. Different control schemes were developed and tried on numerical simulations. These simulations required the mathematical model associated with SCOUT. The modeling considerations demonstrated that SCOUT is a two DOF system, with only one actuator (hip motor). Three different control strategies (polynomial, ramp and saturated ramp controllers) were presented and the experimental results for the implementation of the last two were shown.

## 5.2. Conclusions

An analysis of the theoretical results presented in Chapter 3 and the experimental results (Chapter 4) shows several differences. This disagreement can be explained by the modeling assumptions presented in Chapter 2. There are several factors that are

present in the physical system and were not accounted for in the theoretical model of the system.

One of the effects that we were able to prove to have a significant effect on the results was the toe - floor interaction. The current approach used in the design of walking control algorithms relies critically on the momentum transfer. The momentum transfer is based on the assumption that a pin connection between toe and ground is formed as a result of their impact. Video recordings showed an important slippage between toe and floor. This slippage was minimized by the presence of a rough material, like a carpet, on the floor. The influence of slippage was not as evident on smaller robots, like SCOUT I, but become an important effect on larger robots (SCOUT II). Moreover, the legs were modeled as stiff elements. Nevertheless, the toe material and leg design introduces compliant effects, for which the model did not account. This compliance will also have influence over the assumption of perfect plastic impact between toe and floor. Furthermore, the combined effect of the compliance and slippage can explain the presence of the double stance, whose effect on the dynamics was not considered in the modeling part.

Several other elements influence the experimental results, such as overcoming the friction in the mechanical transmissions. Simulations of the ramp controller considered the hardware limitations on the maximum torque delivered by the hip motors, but did not consider the efficiency of motor, gear or belt transmission.

With all of these un-modeled factors, experimental implementation of both ramp controller and saturated ramp controller was successful. However, the ramp controller is closer to the theoretical expected behaviour, due to lower actuation requirements. Although it takes smaller steps, the superiority of the overall performance recommends this control scheme over the saturated ramp controller.

Consequently, the current approach used in the design of walking gaits, if implemented with proper care, can result in periodic, stable walking motions. However, this approach is vulnerable to slippage problems and un-modeled properties, such as compliance in legs.

## 5.3. Recommendations for Future Work

Simulations for both ramp controller and saturated ramp controller showed that increasing leg length can improve the overall behavior, for example, lower required hip torques, faster steps, etc. Nevertheless, a more in-depth analysis is required.

The implementation of the polynomial controller on SCOUT II could result in successful experiments. Its potential has yet to be tested, and is the only control scheme in which both front and back leg contribute to the forward displacement of the body.

For future control algorithms, significant attention has to be paid to the modeling part. With our conclusions from the experimental work, some of the assumptions made in developing the mathematical model have to be revised. The most important ones are the modeling of toe - floor interaction. In developing future control algorithms, the use of optimization techniques might be successful. These methods will allow the design of control strategies that consider the energy consumption issue, or consider the hardware limitations on available actuator torque.

The conclusions showed that the success of the designed controllers is highly dependent on the closeness between the model and physical system. Currently, SCOUT II is equipped with legs that can be adapted for running experiments, where compliance is an important factor. However, during walking important impacts occur; therefore a more robust leg design should be considered. Furthermore, the slippage of the foot on the floor is a direct result of the interaction between the foot material and floor surface. The use of sticky materials for the leg toes and floor can reduce the slipping effect.

Some work should be put into the experimental software. Different sets of gains are used as a function of the current state, for example, support on back or front legs and double stance. However, in double stance there is a tendency for the legs to work against each other, in order to attain their desired position. Consequently, different sets of gains need to be set on the back legs and front legs for the double stance following the back leg support, and the double stance following front leg support.

The experimental software can accommodate the walking backwards and forwards. However, some work has to be done towards proper gain settings at the switch between walking backwards and forwards.

# REFERENCES

[1] P. R. Bélanger. *Control Engineering: A Modern Approach.* Saunders College Publishing, 1995.

[2] M. Buehler, R. Battaglia, A. Cocosco, G. Hawker, J. Sarkis, and K. Yamazaki. Scout: A simple quadruped that walks, climbs and runs. *Proc. IEEE Int. Conf. Robotics and Automation*, pages 1701–1712, 1998.

[3] P. H. Channon, S. K. Hopkins, and D. T. Pham. Derivation of optimal walking motions for a bipedal walking robot. *Robotica*, 10:165–172, 1992.

[4] E. R. Dunn and R. D. Howe. Towards smooth bipedal walking. *Proc. IEEE Int. Conf. Robotics and Automation*, 3:2489–2494, May 1994.

[5] E. R. Dunn and R. D. Howe. Foot placement and velocity control in smooth bipedal walking. In *Proc. IEEE Int. Conf. Robotics and Automation*, pages 578–583. Minneapolis, MN, Apr 1996.

[6] The Math. Works Inc. *MATLAB Reference Guide.* 1992.

[7] S. Kajita, K. Tani, and A. Kobayashi. Dynamic walk control of a biped robot along the potential energy conserving orbit. In *IEEE Int. Conf. on Intelligent Robots and Systems*, pages 789–794, 1990.

[8] A. Kecskeméthy. *MOBILE.* Graz, Austria, 1996.

[9] QNX Software Systems Ltd. *QNX TCP/IP Users Guide.* 1994.

[10] D. W. Marhefka and D. E. Orin. Gait planning for energy efficiency in walking machines. *Proc. IEEE Int. Conf. Robotics and Automation*, pages 474–180, 1997.

[11] T. McGeer. Stability and control of two-dimensional biped walking. Technical Report IS-TR-88-01, Simon Fraser University, Centre for Systems Science, Sep 1988.

[12] T. McGeer. Dynamics and control of bipedal locomotion. Technical report, School of Engineering Science, Simon Fraser University, Burnaby, BC, January 1990.

[13] T. McGeer. Passive dynamic walking. *Int. J. Robotics Research*, 9(2):62–82, 1990.

[14] J.L. Meriam and L.G. Kraige. *Engineering Mechanics*. John Wiley & Sons Inc., 1992.

[15] H. Miura and I. Shimoyama. Dynamic walk of a biped. *Int. J. Robotics Research*, 3(2):60–74, 1984.

[16] M. H. Raibert. *Legged Robots That Balance*. MIT Press, Cambridge, MA, 1986.

[17] Knowledge Revolution. *Working Model 2D User's Guide*. 1996.

[18] A. Sano and J. Furusho. Realization of natural dynamic walking using the angular momentum information. In *Proc. IEEE Int. Conf. Robotics and Automation*, pages 1476–1481, 1990.

[19] A. C. Smith and M. D. Berkemeier. Passive dynamic qudrupedal walking. *Proc. IEEE Int. Conf. Robotics and Automation*, pages 34–39, April 1997.

# APPENDIX A

# EQUATIONS OF MOTION

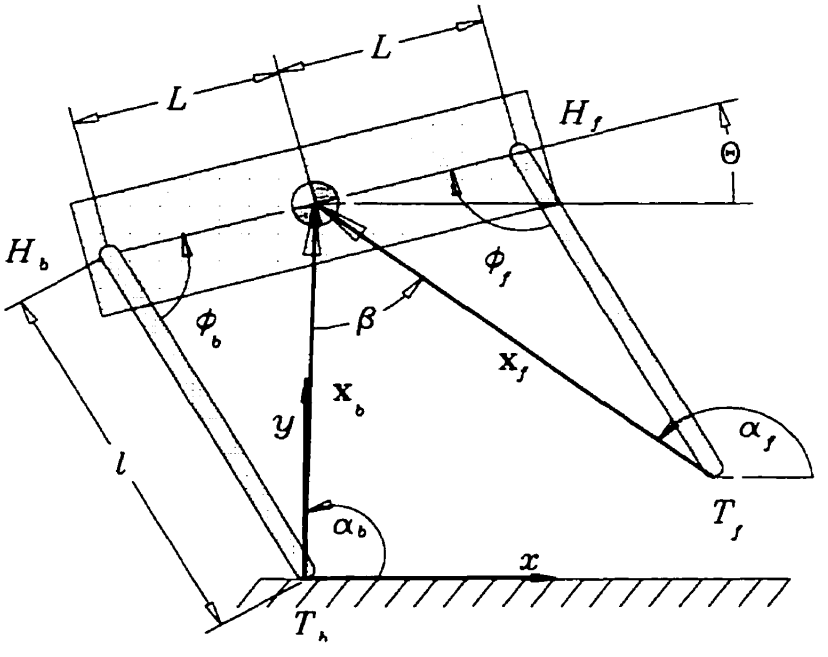


FIGURE A.1. SCOUT model

The notation used in this appendix is the one defined in Tables 2.1 and 2.2 and Figure A.1. The detailed derivation of the equations of motion for the back leg support case

will be presented. Then, using coordinate transformations, it is possible to express the same set of equations for the front leg support phase.

## A.1. Back leg Support

$$\mathbf{x}_b = \begin{bmatrix} -l\cos(\theta-\phi_b)+L\cos\theta \\ -l\sin(\theta-\phi_b)+L\sin\theta \end{bmatrix}; \qquad \dot{\mathbf{x}}_b = \begin{bmatrix} l(\dot\theta-\dot\phi_b)\sin(\theta-\phi_b)-L\dot\theta\sin\theta \\ -l(\dot\theta-\dot\phi_b)\cos(\theta-\phi_b)+L\dot\theta\cos\theta \end{bmatrix}.$$

$$\begin{aligned} \mathrm{T} &= \frac{1}{2}m\dot{\mathbf{x}}_b^T\dot{\mathbf{x}}_b + \frac{1}{2}mr^2\dot\theta^2 \\ &= \frac{1}{2}m\left[[r^2+L^2+l^2-2Ll\cos\phi_b]\dot\theta^2 + l^2\dot\phi_b^2 - 2l[l-L\cos\phi_b]\dot\theta\dot\phi_b\right] \\ \mathrm{V} &= mg[-l\sin(\theta-\phi_b)+L\sin\theta] \\ \mathcal{L} &= \mathrm{T}-\mathrm{V} \end{aligned}$$

$$\begin{aligned} \frac{\partial\mathcal{L}}{\partial\dot\theta} &= m\left[[r^2+L^2+l^2-2Ll\cos\phi_b]\dot\theta - l[l-L\cos\phi_b]\dot\phi_b\right] \\ \frac{\partial\mathcal{L}}{\partial\dot\phi_b} &= m\left[l^2\dot\phi_b - l[l-L\cos\phi_b]\dot\theta\right] \\ \frac{d}{dt}\frac{\partial\mathcal{L}}{\partial\dot\theta} &= m\left[[r^2+L^2+l^2-2Ll\cos\phi_b]\ddot\theta - l[l-L\cos\phi_b]\ddot\phi_b + 2Ll\sin\phi_b\dot\theta\dot\phi_b - Ll\sin\phi_b\dot\phi_b^2\right] \\ \frac{d}{dt}\frac{\partial\mathcal{L}}{\partial\dot\phi_b} &= m\left[l^2\ddot\phi_b - l[l-L\cos\phi_b]\ddot\theta - Ll\dot\theta\dot\phi_b\sin\phi_b\right] \\ \frac{\partial\mathcal{L}}{\partial\theta} &= mg\left[l\cos(\theta-\phi_b)-L\cos\theta\right] \\ \frac{\partial\mathcal{L}}{\partial\phi_b} &= m\left[Ll\sin\phi_b\dot\theta^2 - Ll\sin\phi_b\dot\theta\dot\phi_b - gl\cos(\theta-\phi_b)\right] \end{aligned}$$

So, the non-linear equations of motions are

$$\begin{cases} [r^2 + L^2 + l^2 - 2Ll\cos\phi_b]\ddot{\theta} - l[l - L\cos\phi_b]\ddot{\phi}_b \\ \qquad +2lL\dot{\phi}_b\dot{\theta}\sin\phi_b - Ll\dot{\phi}_b^2\sin\phi_b - gl\cos(\theta - \phi_b) + gL\cos\theta = 0 \\ -l[l - L\cos\phi_b]\ddot{\theta} + l^2\ddot{\phi}_b - lL\dot{\theta}^2\sin\phi_b + gl\cos(\theta - \phi_b) = \tau_b/m. \end{cases} \tag{A.1}$$

Let $x = [\ \theta\ \dot{\theta}\ \phi_b\ \dot{\phi}_b]^T$ be the state vector. Then eq. (A.1) can be written in state space form

$$\begin{cases} \dot{x}_1 &= x_2 \\ \dot{x}_2 &= \frac{1}{r^2+L^2\sin^2 x_3}[L(l - L\cos x_3)x_2^2\sin x_3 + Llx_4^2\sin x_3 \\ &\quad -2lLx_2x_4\sin x_3 + gL\cos x_3\cos(x_1 - x_3) - gL\cos x_1 \\ &\quad +\frac{1}{l}[l - L\cos x_3]\frac{\tau_b}{m}] \\ \dot{x}_3 &= x_4 \\ \dot{x}_4 &= \frac{l - L\cos x_3}{l(r^2+L^2\sin^2 x_3)}[L(l - L\cos x_3)x_2^2\sin x_3 + Llx_4^2\sin x_3 \\ &\quad -2lLx_2x_4\sin x_3 + gL\cos x_3\cos(x_1 - x_3) - gL\cos x_1 \\ &\quad +\frac{1}{l}[l - L\cos x_3]\frac{\tau_b}{m}] + \frac{L}{l}x_2^2\sin x_3 - \frac{g}{l}\cos(x_1 - x_3) + \frac{1}{l^2}\frac{\tau_b}{m}. \end{cases}$$

Using the technique presented in [**1**] and the linearization point $x^* = [\,0\ 0\ \pi/2\ \dot{\phi}_i]^T$, the linear set of equations for back leg support, in state space form is

$$\begin{cases} \dot{x}_1 &= x_2 \\ \dot{x}_2 &= \frac{Ll\dot{\phi}_i^2}{r^2+L^2} - \frac{2lL\dot{\phi}_i}{r^2+L^2}x_2 + \frac{gL^2}{l(r^2+L^2)}(x_3 - \frac{\pi}{2}) \\ &\quad +\frac{2Ll\dot{\phi}_i}{r^2+L^2}(x_4 - \dot{\phi}_i) + \frac{1}{r^2+L^2}(\frac{\tau_b}{m} - gL) \\ \dot{x}_3 &= x_4 \\ \dot{x}_4 &= \frac{Ll\dot{\phi}_i^2}{r^2+L^2} + \frac{gL}{l^2} - \frac{g}{l}x_1 - \frac{2lL\dot{\phi}_i}{r^2+L^2}x_2 \\ &\quad +\frac{g(2L^2+r^2)}{l(r^2+L^2)}(x_3 - \frac{\pi}{2}) + \frac{2Ll\dot{\phi}_i}{r^2+L^2}(x_4 - \dot{\phi}_i) \\ &\quad +[\frac{1}{r^2+L^2} + \frac{1}{l^2}](\frac{\tau_b}{m} - gL). \end{cases}$$

## A.2. Front leg Support

From eq. (A.1) using the simple coordinate transformation

$$\begin{cases} \theta \longrightarrow \theta - \pi \\ \phi_b \longrightarrow 2\pi - \phi_f \end{cases}$$

the non-linear equations of motion are

$$\begin{cases} [r^2 + L^2 + l^2 - 2Ll\cos\phi_f]\ddot{\theta} + l[l - L\cos\phi_f]\ddot{\phi}_f + 2lL\dot{\phi}_f\dot{\theta}\sin\phi_f + Ll\dot{\phi}_f^2\sin\phi_f \\ \qquad\qquad +gl\cos(\theta+\phi_f) - gL\cos\theta = 0 \\ l[l - L\cos\phi_f]\ddot{\theta} + l^2\ddot{\phi}_f - lL\dot{\theta}^2\sin\phi_f + gl\cos(\theta+\phi_f) = \tau_f/m. \end{cases}$$

Let $x = [\ \theta\ \dot{\theta}\ \phi_f\ \dot{\phi}_f]^T$ be the state vector. Then eq. A.2 can be written in state space form

$$\begin{cases} \dot{x}_1 &= x_2 \\ \dot{x}_2 &= \frac{1}{r^2+L^2\sin^2 x_3}[-L(l - L\cos x_3)x_2^2\sin x_3 - Llx_4^2\sin x_3 \\ &\quad -2lLx_2x_4\sin x_3 - gL\cos x_3\cos(x_1+x_3) + gL\cos x_1 \\ &\quad -\frac{1}{l}[l - L\cos x_3]\frac{\tau_f}{m}] \\ \dot{x}_3 &= x_4 \\ \dot{x}_4 &= -\frac{l-L\cos x_3}{l(r^2+L^2\sin^2 x_3)}[-L(l - L\cos x_3)x_2^2\sin x_3 - Llx_4^2\sin x_3 \\ &\quad -2lLx_2x_4\sin x_3 - gL\cos x_3\cos(x_1+x_3) + gL\cos x_1 \\ &\quad -\frac{1}{l}[l - L\cos x_3]\frac{\tau_f}{m}] + \frac{L}{l}x_2^2\sin x_3 - \frac{g}{l}\cos(x_1+x_3) + \frac{1}{l^2}\frac{\tau_f}{m}. \end{cases}$$

Again using the technique presented in [**1**] and the linearization point $x^* = [\ 0\ 0\ \pi/2\ \dot{\phi}_i]^T$, the linear set of equations for front leg support. in state space form is

$$
\begin{cases}
\dot{x}_1 &= x_2 \\
\dot{x}_2 &= -\frac{Ll\dot{\phi}_i^2}{r^2+L^2} - \frac{2lL\dot{\phi}_i}{r^2+L^2}x_2 + \frac{gL^2}{l(r^2+L^2)}(x_3 - \frac{\pi}{2}) \\
&\quad -\frac{2Ll\dot{\phi}_i}{r^2+L^2}(x_4 - \dot{\phi}_i) - \frac{1}{r^2+L^2}(\frac{\tau_f}{m} - gL) \\
\dot{x}_3 &= x_4 \\
\dot{x}_4 &= \frac{Ll\dot{\phi}_i^2}{r^2+L^2} + \frac{gL}{l^2} + \frac{g}{l}x_1 + \frac{2lL\dot{\phi}_i}{r^2+L^2}x_2 \\
&\quad +\frac{g(2L^2+r^2)}{l(r^2+L^2)}(x_3 - \frac{\pi}{2}) + \frac{2Ll\dot{\phi}_i}{r^2+L^2}(x_4 - \dot{\phi}_i) \\
&\quad +[\frac{1}{r^2+L^2} + \frac{1}{l^2}](\frac{\tau_f}{m} - gL).
\end{cases}
$$

# APPENDIX B

# IMPACT MODEL

## B.1. Impact equations based on double pendulum model

**B.1.1. Back Leg Impact.** With reference to the notation presented in Figure A.1, and the definition of the angular momentum given in eq. (2.7), the angular moment just before and immediately after the impact, with respect to the back leg toe are

$$\begin{aligned} H^- &= I\dot{\theta}^{B-} + m(x_b\dot{y}_f - \dot{x}_f y_b) \\ &= m\Big[[l[-l\cos(\phi_b^B + \phi_f^B) + L\cos\phi_f^B] + r^2 - L^2 + lL\cos\phi_b^B]\dot{\theta}^{B-} \\ &\quad + l[-l\cos(\phi_b^B + \phi_f^B) + L\cos\phi_f^B]\dot{\phi_f}^{B-}\Big] \\ H^+ &= I\dot{\theta}^{B+} + m(x_b\dot{y}_b - \dot{x}_b y_b) \\ &= m\Big[[l[l - L\cos\phi_b^B] + r^2 + L^2 - lL\cos\phi_b^B]\dot{\theta}^{B+} - l[l - L\cos\phi_b^B]\dot{\phi}_b^{B+}\Big]. \end{aligned}$$

With $H^- = H^+$, the impact is governed by

$$[l[-l\cos(\phi_b^B+\phi_f^B)+L\cos\phi_f^B]+r^2-L^2+lL\cos\phi_b^B]\dot{\theta}^{B-}$$
$$+l[-l\cos(\phi_b^B+\phi_f^B)+L\cos\phi_f^B]\dot{\phi_f}^{B-}=$$
$$[l[l-L\cos\phi_b^B]+r^2+L^2-lL\cos\phi_b^B]\dot{\theta}^{B+}-l[l-L\cos\phi_b^B]\dot{\phi}_b^{B+}.$$

**B.1.2. Front Leg impact.** Again, with reference to the notation presented in Figure A.1, and the definition of the angular momentum given in eq. (2.7), the momenta just before and immediately after the impact, with respect to the front leg toe are

$$\begin{aligned}
H^- &= I\dot{\theta}^{F-}+m(x_f\dot{y}_b-\dot{x}_by_f)\\
&= m\Big[[l[-l\cos(\phi_b^F+\phi_f^F)+L\cos\phi_b^F]+r^2-L^2+lL\cos\phi_f^F]\dot{\theta}^{F-}\\
&\quad -l[-l\cos(\phi_b^F+\phi_f^F)+L\cos\phi_b^F]\dot{\phi_b}^{F-}\Big]\\
H^+ &= I\dot{\theta}^{F+}+m(x_f\dot{y}_f-\dot{x}_fy_f)\\
&= \Big[[l[l-L\cos\phi_f^F]+r^2+L^2-lL\cos\phi_f^F]\dot{\theta}^{F+}+l[l-L\cos\phi_f^F]\dot{\phi}_f^{F+}\Big].
\end{aligned}$$

So the impact is governed by :

$$[l[-l\cos(\phi_b^F+\phi_f^F)+L\cos\phi_b^F]+r^2-L^2+lL\cos\phi_f^F]\dot{\theta}^{F-}$$
$$-l[-l\cos(\phi_b^F+\phi_f^F)+L\cos\phi_b^F]\dot{\phi_b}^{F-}=$$
$$[l[l-L\cos\phi_f^F]+r^2+L^2-lL\cos\phi_f^F]\dot{\theta}^{F+}+l[l-L\cos\phi_f^F]\dot{\phi}_f^{F+}.$$

## B.2. Impact Equations Based on Virtual Leg Model

In this section we will use the notations presented on Figure A.1. The vector along the back or front virtual leg

$$\mathbf{x}_{b,f} = \begin{bmatrix} x_{b,f} \\ y_{b,f} \end{bmatrix} = \begin{bmatrix} l_{b,f}\cos\alpha_{b,f} \\ l_{b,f}\sin\alpha_{b,f} \end{bmatrix}; \qquad \dot{\mathbf{x}}_{b,f} = \begin{bmatrix} \dot{x}_{b,f} \\ \dot{y}_{b,f} \end{bmatrix} \begin{bmatrix} \dot{l}_{b,f}\cos\alpha_{b,f} - l_{b,f}\dot{\alpha}_{b,f}\sin\alpha_{b,f} \\ \dot{l}_{b,f}\sin\alpha_{b,f} + l_{b,f}\dot{\alpha}_{b,f}\cos\alpha_{b,f} \end{bmatrix}$$

**B.2.1. Back Leg Impact.** Again, starting from eq. (2.7), the angular momenta just before and immediately after the back leg impact with the ground are

$$\begin{aligned} H^- &= I\dot{\theta}^{B-} + m[x_b\dot{y}_f - y_b\dot{x}_f] \\ &= m\left[r^2\dot{\theta}^{B-} - l_b^B\dot{l}_f sin\beta^B + l_b^B l_f^B\dot{\alpha}_f^{B-}\cos\beta^B\right] \\ H^+ &= I\dot{\theta}^{B+} + m[x_b\dot{y}_b - y_b\dot{x}_b] \\ &= m[r^2\dot{\theta}^{B+} + (l_b^B)^2\dot{\alpha}_b^{B+}]. \end{aligned}$$

In the above equation we made use of $\beta^B = \alpha_f^B - \alpha_b^B$. Using trigonometric identities it is possible to show that

$$\dot{\alpha}_{b,f} = \dot{\theta} - C_{b,f}\dot{l}_{b,f} \tag{B.1}$$

where $C_{b,f}$ is a constant that depends only on the geometry of the system, that is

$$C_{b,f} = \frac{1}{4l_{b,f}L^2}\frac{3L^2 + (l_{b,f})^2}{\sqrt{1 - (\frac{5}{4} - (\frac{l_{b,f}}{2L})^2)^2}}. \tag{B.2}$$

Given $H^- = H^+$, the conservation of angular momentum is given by

$$\begin{aligned} &[r^2 + l_b^B l_f^B\cos\beta^B]\dot{\theta}^{B-} + [l_b^B\sin\beta^B - C_f^B l_b^B l_f^B\cos\beta^B]\dot{l_f}^{B-} \\ &\qquad = [r^2 + (l_b^B)^2]\dot{\theta}^{B+} - C_b^B(l_b^B)^2\dot{l_b}^{B+}. \end{aligned} \tag{B.3}$$

From eq. (B.3), the velocity of the front virtual leg, just before back leg impact, can be expressed as,

$$\dot{l}_f^{B-} = \frac{[r^2 + l_b^B l_f^B \cos\beta^B]\dot{\theta}^{B-} - [r^2 + (l_b^B)^2]\dot{\theta}^{B+}}{C_f^B l_b^B l_f^B \cos\beta^B - l_b^B \sin\beta^B}. \tag{B.4}$$

Therefore, in eq. (3.4),

$$\begin{aligned} c_1 &= \frac{[r^2 + l_b^B l_f^B \cos\beta^B]}{C_f^B l_b^B l_f^B \cos\beta^B - l_b^B \sin\beta^B} \\ c_2 &= \frac{r^2 + (l_b^B)^2}{C_f^B l_b^B l_f^B \cos\beta^B - l_b^B \sin\beta^B}. \end{aligned} \tag{B.5}$$

**B.2.2. Front Leg Impact.** From the basic momentum transfer relation shown in eq. (2.7) and eq. (B.2)

$$\begin{aligned} H^- &= mr^2\dot{\theta}^{F-} + m[x_f\dot{y}_b - y_f\dot{x}_b] \\ &= m\left[r^2\dot{\theta}^{F-} - \dot{l}_b^F l_f^F sin\beta^F + l_b^F l_f^F \dot{\alpha}_b^{F-}\cos\beta^F\right] \\ H^+ &= mr^2\dot{\theta}^{F+} + m[x_f\dot{y}_f - y_f\dot{x}_f] \\ &= m\left[r^2\dot{\theta}^{F+} + (l_f^F)^2\dot{\alpha}_f^{F+}\right]. \end{aligned}$$

Using the results presented in Sections B.1 and B.2 the conservation of angular momentum is expressed as

$$\begin{aligned} [r^2 + l_b^F l_f^F \cos\beta^F]\dot{\theta}^{F-} - [l_f^F \sin\beta^F + C_b^F l_b^F l_f^F \cos\beta^F]\dot{l_b}^{F-} = \\ [r^2 + (l_f^F)^2]\dot{\theta}^{F+} - C_f^F (l_f^F)^2 \dot{l_f}^{F+} \end{aligned} \tag{B.6}$$

The velocity of the virtual back leg just before front impact can be expressed as:

$$\dot{l}_b^{F-} = \frac{[r^2 + l_b^F l_f^F \cos\beta^F]\dot{\theta}^{F-} - [r^2 + (l_f^F)^2]\dot{\theta}^{F+}}{l_f^F \sin\beta^F + C_b^F l_b^F l_f^F \cos\beta^F} \tag{B.7}$$

Therefore, in eq. (3.3)

$$c_3 = \frac{r^2 + l_b^F l_f^F \cos\beta^F}{l_f^F \sin\beta^F + C_b^F l_b^F l_f^F \cos\beta^F} \tag{B.8}$$

$$c_4 = \frac{r^2 + (l_f^F)^2}{l_f^F \sin\beta^F + C_b^F l_b^F l_f^F \cos\beta^F}. \tag{B.9}$$

## Document Log:

Manuscript Version 1 — June 1, 1998

Typeset by $\mathcal{A}\mathcal{M}\mathcal{S}$-LaTeX — 1 October 1998

ANCA ELENA COCOSCO

CENTER FOR INTELLIGENT MACHINES, MCGILL UNIVERSITY, MONTRÉAL (QUÉBEC) H3A 2A7, CANADA, 3480 UNIVERSITY ST., *Tel.* : (514) 398-8054

*E-mail address*: anca@cim.mcgill.ca

Typeset by $\mathcal{A}\mathcal{M}\mathcal{S}$-LaTeX